$W^{\pm}Z$ production at NNLO QCD and NLO EW matched to parton showers with MiNNLO_PS

Jonas M. Lindert,[a] **Daniele Lombardi,**[b] **Marius Wiesemann,**[b] **Giulia Zanderighi**[b,c] **and Silvia Zanoli**[b]

[a]*Department of Physics and Astronomy, University of Sussex,*
Brighton, BN1 9QH, U.K.

[b]*Max-Planck-Institut für Physik,*
Föhringer Ring 6, 80805 München, Germany

[c]*Physik-Department, Technische Universität München,*
James-Franck-Strasse 1, 85748 Garching, Germany

E-mail: lindert@sussex.ac.uk, lombardi@mpp.mpg.de,
wieseman@mpp.mpg.de, zanderi@mpp.mpg.de, zanoli@mpp.mpg.de

ABSTRACT: We consider $W^{\pm}Z$ production in hadronic collisions and present high-precision predictions in QCD and electroweak (EW) perturbation theory matched to parton showers. To this end, we match next-to-next-to-leading order QCD corrections to parton showers using the MiNNLO_PS method and consistently combine them with next-to-leading order EW corrections matched to parton showers. This is the first time such accuracy in the event generation is achieved for any collider process, and we study in detail the impact of different choices in the combination of QCD and EW corrections as well as QCD and QED showers. Spin correlations, interferences and off-shell effects are retained by considering the full leptonic processes $pp \to \ell^+\ell^-\ell'^{\pm}\nu'_{\ell}$ with $\ell' \neq \ell$ and $\ell' = \ell$ without approximations, and the matching to QED radiation is performed preserving the resonance structure of the process. We find that NNLO QCD predictions including QCD and QED shower effects provide a very good approximation in the bulk-region of the phase space, while EW effects become increasingly important in the high-energy tails of kinematic distributions. Our default predictions are in excellent agreement with recent ATLAS data.

Contents

1 Introduction

Among the major theoretical challenges for today's physics program at CERN's Large Hadron Collider (LHC) are precision simulations of proton-proton reactions based on calculations in QCD and EW perturbation theory at the highest possible order. The high demand for such accurate predictions is the result of the remarkable performance of the LHC experiments, which keep decreasing the experimental uncertainties of various inclusive and differential cross-section measurements. Moreover, without clear hints for new physics at the LHC thus far, data-theory comparisons at high precision have become a promising path towards the observation of deviations from the Standard Model (SM) picture.

The class of processes where a pair of vector bosons (decaying to leptons) is produced represents a highly relevant set of LHC reactions in these endeavours. Not only do these processes provide direct access to trilinear gauge couplings, which are often modified or added as new contributions with respect to the SM Lagrangian in various beyond-the-SM (BSM) theories, they also yield a central test of the gauge-symmetry structure of EW interactions within the SM, as any small deviation from the expected rates or shapes of distributions could be a signal of new physics. In this context, $W^{\pm}Z$ production is particularly interesting due its relatively large cross section and clean experimental signature, which allows very

accurate experimental measurements of this process at the LHC. Moreover, $W^\pm Z$ production holds a special place in BSM searches, both as signal and as background. Indeed, even within the SM $W^\pm Z$ production features a trilinear gauge coupling that enters already at tree-level. On the other hand, the $W^\pm Z$ process yields an important SM background in many BSM resonance searches, such as for supersymmetric particles (see e.g. ref. [1]).

Measurements of the $W^\pm Z$ cross section have been performed both at the Tevatron [2, 3] and at the LHC for centre-of-mass energies of 7 TeV [4, 5], 8 TeV [5, 6] and 13 TeV [7–10]. On the theory side, next-to-leading-order (NLO) predictions in QCD for $W^\pm Z$ production were obtained long ago [11–15]. Corresponding results for polarized $W^\pm Z$ production became available only recently in the double-pole approximation [16]. The computation of the $W^\pm Z$+jet cross section at NLO QCD was presented in ref. [17]. The first next-to-NLO (NNLO) QCD accurate predictions were obtained for the inclusive $W^\pm Z$ cross section in ref. [18], which were later extended to the fully differential predictions including leptonic decays in ref. [19]. The computation of NNLO QCD corrections are publicly available in the parton-level Monte Carlo framework MATRIX [20] and MCFM [21]. In the MATRIX framework also the effect of the b-space resummation of large logarithmic terms at small transverse momenta of the $W^\pm Z$ system up to next-to-next-to-leading logarithmic accuracy (NNLL) has been incorporated [22]. More recently, the MATRIX+RADISH framework was introduced [20, 23–27], which makes NNLO+N³LL predictions for the $W^\pm Z$ transverse momentum, NNLO+NNLL predictions for the transverse momentum of the leading jet, as well as their joint resummation at NNLO+NNLL publicly available. NLO EW corrections to $W^\pm Z$ production are known for both on-shell $W^\pm Z$ production [28, 29] and including off-shell leptonic decays [30]. The NLO EW predictions have been combined with NNLO QCD corrections and are publicly available as provided by MATRIX+OPENLOOPS [31].

However, apart from idealised parton-level perturbative calculations at higher orders, full-fledged Monte-Carlo simulations that include higher-order corrections are becoming more and more important, as they pair a realistic modelling of LHC events, including effects from QCD and QED parton showers, hadronization and multiple-parton interactions, with higher-order perturbative information. To this end, the inclusion of NNLO QCD corrections in parton-shower simulations (NNLO+PS) has been a very active research topic in the past ten years, which has led to the formulation of various approaches [32–36] and ultimately to a remarkable progress in NNLO+PS calculations for a number of colour-singlet production processes, including H [35–38], $Z/W^\pm$ [34–36, 39–41], $ZH/W^\pm H$ [42–46], $\gamma\gamma$ [47, 48], $Z\gamma$ [49, 50], ZZ [51, 52], and W^+W^- [53, 54]. With top-quark pair production even the first production process with colour charges in the final state has been computed at NNLO+PS [55, 56]. Recently, also the matching of NLO EW corrections to QED and QCD parton showers has been considered for massive diboson processes [57, 58]. In order to ensure a consistent off-shell description in ref. [57] the matching had to be performed in a resonance-aware fashion as provided by the POWHEG-BOX-RES framework [59].

In this paper we present the first NNLO+PS calculation for $W^\pm Z$ production in QCD, and we combine these results with NLO EW corrections matched consistently to parton showers. More precisely, we consider the full process that leads to three leptons and one neutrino, $pp \to \ell'^\pm \nu_{\ell'} \ell^+ \ell^- + X$, in both the same-flavour ($\ell' = \ell$) and the different-

flavour ($\ell' \neq \ell$) channel, taking into account all non-resonant, single-resonant and double-resonant components with all interference effects, spin correlations and off-shell effects in the complex-mass scheme [60], and we combine NNLO QCD and NLO EW corrections properly matched to QCD and QED parton showers. We validate our predictions against the corresponding fixed-order calculations, and we study various possible schemes for the combination of QCD and EW corrections. These different schemes not only distinguish between additive and multiplicative combinations, but also avoid the double-counting of QCD and QED radiation effects in different ways, thereby differing by all-order terms that are beyond accuracy. We note that among all diboson processes $W^\pm Z$ production offers a valuable application to perform this study. In particular, unlike charge-neutral diboson production, the $W^\pm Z$ process does not involve a loop-induced gluon fusion channel, which receives sizeable higher-order QCD corrections that are crucial to obtain accurate predictions [61–67]. $W^\pm Z$ production does also not feature photon-induced subprocesses at the Born level. Our calculation is performed and implemented within POWHEG-BOX-RES and will be made publicly available.

This manuscript is organized as follows: in section 2 we describe our calculation including the relevant information on the process (section 2.1), on the MiNNLO$_{\rm PS}$ method and its practical implementation to obtain a $W^\pm Z$ NNLO+PS QCD generator (section 2.2), on the NLO+PS EW implementation (section 2.3), on constraining QCD and QED shower radiation that is necessary to preserve the accuracy of the predictions (section 2.4) and on the combination of QCD and EW corrections (section 2.5). In section 3 phenomenological results are presented, where we first discuss our input settings (section 3.1) and subsequently validate our NNLO QCD and NLO EW accurate event simulations against fixed-order results (section 3.2), compare different QCD and EW combination schemes (section 3.3), and finally present a comparison of our best predictions to recent ATLAS data (section 3.4). We conclude in section 4.

2 Outline of the calculation

2.1 Description of the process and notation

We consider the process

$$pp \to \ell'^{\pm}\nu_{\ell'}\ell^{+}\ell^{-} + X \,, \tag{2.1}$$

for any combination of massless leptons $\ell, \ell' \in \{e, \mu, \tau\}$ with both different flavours $\ell \neq \ell'$ and same flavours $\ell = \ell'$. All possible same-flavour and different-flavour lepton combinations have been implemented in the Monte Carlo generator that will be made publicly available within POWHEG-BOX-RES in the near future. Resonant and non-resonant topologies leading to this process, off-shell effects, interferences and spin correlations are taken into account. At LO $W^\pm Z$ production is quark induced and of $\mathcal{O}(\alpha^4)$, where α denotes the electroweak coupling. In this counting the leptonic decays of the vector bosons are included. Sample LO diagrams are shown in figure 1, including t-channel, s-channel and Drell-Yan type contributions. While at higher orders in QCD perturbation theory all combinations of partons in the initial state contribute to the process, due to charge conservation no
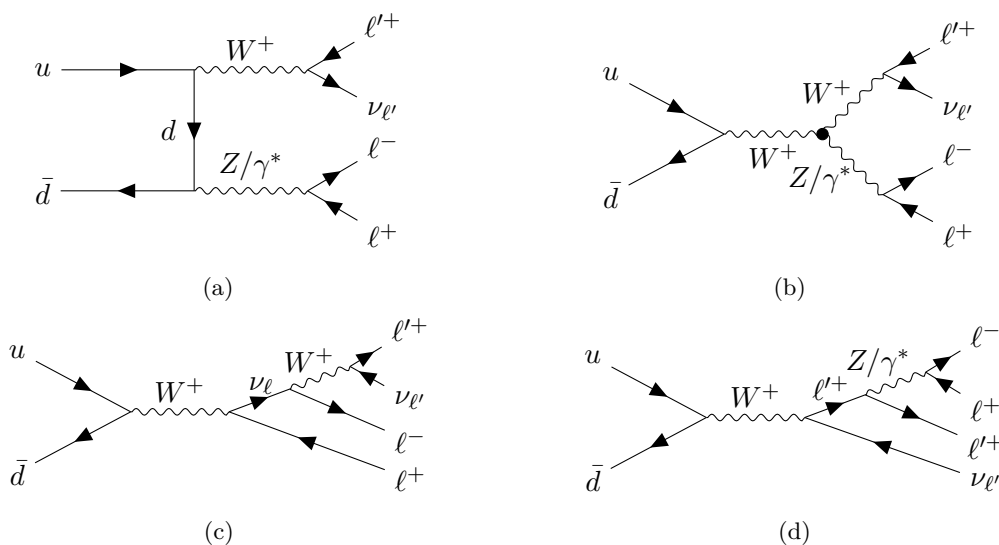
Figure 1. Sample LO diagrams for (a) t-channel W^+Z production, (b) s-channel W^+Z production and (c,d) DY-type W^+Z production channels. The corresponding diagrams for W^-Z production can be obtained via charge conjugation.

additional large $\mathcal{O}(\alpha^4\alpha_s^2)$ contribution of loop-induced gluon-fusion type is present for the process at hand, unlike for the production of charge-neutral diboson systems. However, $W^\pm Z$ production is subject to the so-called radiation zero effect at LO [68], which is caused by the vanishing of the leading helicity amplitudes in some kinematic configurations. This fact renders the LO prediction of the process unreliable, as higher-order corrections become particularly important and large. Consequently, even the NNLO corrections are still of the order of 10–15% [18]. Sample diagrams that contribute at NLO QCD, i.e. $\mathcal{O}(\alpha^4\alpha_s)$, and at NNLO QCD, i.e. $\mathcal{O}(\alpha^4\alpha_s^2)$, can be found in figure 3 of ref. [31].

As far as EW corrections are concerned, we consider contributions up to $\mathcal{O}(\alpha^5)$. At this order virtual corrections enter only through the $q\bar{q}$ channel and involve one-loop diagrams with various combinations of W-bosons, Z-bosons, photons, Higgs bosons, and fermions (including heavy quarks) in the loop. In our calculation real radiation contributions at NLO EW correspond to photon radiation. Representative Feynman diagrams can be found in figure 4 of ref. [31]. Up to the perturbative order under consideration no photon-photon induced contributions appear. There are in principle photon-quark induced contributions with an additional quark in the final state. The computation of such configurations are currently not supported by POWHEG-BOX-RES. Furthermore, since the photon flux in the proton is suppressed by an additional relative $O(\alpha)$ times a collinear logarithm L, we do not consider these photon-quark channels in our computation as they would enter at $\mathcal{O}(\alpha^6 L)$. We note however that, as shown in ref. [30], these channels can yield significant contributions in various high-energy tails driven by configurations where the initial-state photon couples directly to a t-channel W-boson propagator. Therefore, in the future they should be considered also in parton-shower matched predictions. Nevertheless, as discussed in ref. [31] such photon-induced channels should be combined in a purely additive way with

QCD higher-order corrections for the $q\bar{q}$ channels. As a result, those contributions can be implemented independently from the present calculation and added to it incoherently in the future.

Our calculation involves all contributions to NNLO in QCD and the discussed ones to NLO EW including their subsequent matching to QCD and QED parton showers. The NNLO QCD and NLO EW parton-shower matched predictions are obtained independently and then combined based on appropriate prescriptions that will be discussed in section 2.5. In order to simplify the notation we introduce the labels $\mathrm{NNLO_{QCD}}$ and $\mathrm{NLO_{EW}}$ for the fixed-order predictions, and correspondingly $\mathrm{NNLO_{QCD}}+\mathrm{PS}$ and $\mathrm{NLO_{EW}}+\mathrm{PS}$ for their matching to the shower. Where nothing is specified, the parton shower includes both QCD and QED radiation. An appropriate notation is introduced in section 3.3 when predictions combined with only QCD or only QED showering are considered.

2.2 MiNNLO$_{PS}$ method and NNLO$_{QCD}$+PS implementation

Our implementation of the $\mathrm{NNLO_{QCD}}+\mathrm{PS}$ generator for $W^{\pm}Z$ production relies on the MiNNLO$_{PS}$ method. MiNNLO$_{PS}$ was originally formulated and applied to $2 \to 1$ processes [35, 36] and later extended to generic colour-singlet processes [49], and to heavy-quark pair production [55, 56]. We refer to the respective publications for a detailed description of the method, and here instead sketch the main ideas and salient features in a simplified notation.

The matching of NNLO corrections with a parton shower for a system F of colour-singlet particles in the MiNNLO$_{PS}$ method proceeds in three steps: first, in Step I, F in association with one light parton is generated at NLO inclusively over the second radiation via Powheg [69–72]. Second, Step II includes higher-order corrections and an appropriate Sudakov form factor such that the cross section remains finite in the limit where the light partons become unresolved, and the simulation is rendered NNLO accurate for inclusive F production. Third, in Step III the second radiated parton is generated exclusively through Powheg (accounted for inclusively in Step I) and subsequent emissions are generated through the appropriately restricted parton shower. Given that the emissions are correctly ordered in p_T (when using p_T-ordered showers) and the Sudakov form factor in Step II matches the leading logarithms resummed by the parton shower, MiNNLO$_{PS}$ preserves the (leading logarithmic) accuracy of the parton shower.

Symbolically, the fully differential MiNNLO$_{PS}$ cross section can be written as a Powheg calculation for F plus one light parton (FJ), while including NNLO accuracy for F production through a modification of the standard Powheg $\bar{B}$ function:

$$\mathrm{d}\sigma_{\mathrm{F}}^{\mathrm{MiNNLO_{PS}}} = \mathrm{d}\Phi_{\mathrm{FJ}}\,\bar{B}^{\,\mathrm{MiNNLO_{PS}}} \times \left\{ \Delta_{\mathrm{pwg}}(\Lambda_{\mathrm{pwg}}) + \mathrm{d}\Phi_{\mathrm{rad}}\Delta_{\mathrm{pwg}}(p_{\mathrm{T,rad}})\frac{R_{\mathrm{FJ}}}{B_{\mathrm{FJ}}} \right\}, \qquad (2.2)$$

where the modified $\bar{B}$ function $\bar{B}^{\,\mathrm{MiNNLO_{PS}}}$ reads

$$\bar{B}^{\,\mathrm{MiNNLO_{PS}}} = e^{-S}\left\{ \frac{\mathrm{d}\sigma_{\mathrm{FJ}}^{(1)}}{\mathrm{d}\Phi_{\mathrm{FJ}}}\big(1+S^{(1)}\big) + \frac{\mathrm{d}\sigma_{\mathrm{FJ}}^{(2)}}{\mathrm{d}\Phi_{\mathrm{FJ}}} + \big(D - D^{(1)} - D^{(2)}\big) \times F^{\mathrm{corr}} \right\}. \qquad (2.3)$$

In eq. (2.2) Δ_{pwg} denotes the Powheg Sudakov form factor, having a default cutoff of $\Lambda_{\mathrm{pwg}} = 0.89\,\mathrm{GeV}$, while Φ_{rad} and $p_{\mathrm{T,rad}}$ are the phase space and the transverse momentum

of the second radiation (i.e. the real radiation with respect to FJ), respectively. The squared tree-level matrix elements for FJ production and FJJ production are $B_{\rm FJ}$ and $R_{\rm FJ}$, and $\Phi_{\rm FJ}$ indicates the FJ phase space. In eq. (2.3) $d\sigma_{\rm FJ}^{(1,2)}$ denote the LO and NLO differential FJ cross sections and e^{-S} is the Sudakov form factor in the F transverse momentum ($p_{\rm T}$), with $S^{(1)}$ being the $\mathcal{O}(\alpha_s)$ term in the expansion of its exponent. The last term of the $\bar{B}$ function, which is of order $\alpha_s^3(p_{\rm T})$, adds the relevant (singular) contributions necessary to reach NNLO accuracy [35], with regular contributions in $p_{\rm T}$ being subleading at this order.

The function D, which includes the relevant singular terms in $p_{\rm T}$, is derived from a suitable modification of the $p_{\rm T}$ resummation formula, as explained in section 4 of ref. [35],

$$d\sigma_{\rm F}^{\rm res} = \frac{{\rm d}}{{\rm d}p_{\rm T}} \left\{ e^{-S} \mathcal{L} \right\} = e^{-S} \underbrace{\left\{ -S'\mathcal{L} + \mathcal{L}' \right\}}_{\equiv D}, \tag{2.4}$$

where $\mathcal{L}$ denotes the luminosity factor up to NNLO, including the convolution of the collinear coefficient functions with the parton distribution functions (PDFs) and the squared hard-virtual matrix elements for F production. Note that here we do not truncate eq. (2.2) at α_s^3 by evaluating $\left(D - D^{(1)} - D^{(2)} \right) = D^{(3)} + \mathcal{O}(\alpha_s^4)$ as it was done in the original formulation of MiNNLO$_{\rm PS}$ in ref. [35]. Instead, we preserve the total derivative in eq. (2.4) by keeping the respective terms beyond $\mathcal{O}(\alpha_s^3)$, which was proposed in ref. [36] as a way to achieve a better agreement with fixed-order NNLO results by accounting for subleading logarithmic contributions. Finally, the factor $F^{\rm corr}$ in eq. (2.3) ensures that $\left(D - D^{(1)} - D^{(2)} \right)$, which has Born-like kinematics, is appropriately spread in the FJ phase space when generating FJ Powheg events [35].

We have implemented our MiNNLO$_{\rm PS}$ generator for $W^\pm Z$ production in the Powheg-Box-Res framework [59]. Since no generator for $W^\pm Z$+jet production was available, we have first implemented this process in the Powheg-Box-Res framework. In a second step, we have upgraded this implementation by means of the MiNNLO$_{\rm PS}$ method to achieve NNLO QCD accuracy for $W^\pm Z$ production, using the general MiNNLO$_{\rm PS}$ implementation for colour-singlet production developed in ref. [49]. As far as the physical amplitudes are concerned, our calculation relies on OpenLoops [73–75] for all tree-level and one-loop amplitudes via the interface developed in ref. [76], while for the two-loop amplitudes VVamp [77, 78] is used through the interface to Matrix [20] developed in ref. [49]. As for ZZ production in ref. [52], we exploit the possibility of reweighting events at the generation level (stage 4) to include the two-loop contribution, since the evaluation of the two-loop helicity amplitudes for massive diboson processes is known to be computationally very demanding. This procedure substantially reduces the computing time of the process, since the two-loop contribution is just included at generation level and evaluated once per (accepted) event. This feature of the code can be controlled by appropriate settings of the `run_mode` flag, as described in detail in ref. [52].

Our calculation involves the evaluation of several convolutions with the PDFs, for which we employ HOPPET [79]. More precisely, the PDFs are read through the LHAPDF interface [80] and evolved internally by HOPPET [79] as described in ref. [35]. The evaluation of the polylogarithms entering the collinear coefficient functions is done through the HPLOG package [81].

In the following, we briefly summarize the most relevant technical settings that we have used to generate $\mathrm{NNLO_{QCD}+PS}$ events for $W^\pm Z$ production: for more detailed information on those settings we refer the reader to refs. [36, 56]. At large p_T, spurious contributions from higher-order logarithmic corrections are avoided by using a modified logarithm introduced in eq. (4.15) of ref. [56]. For the renormalization and factorization scales we employ the typical $\mathrm{MiNNLO_{PS}}$ scale setting at small p_T, which is defined in eq. (14) of ref. [36], while in the NLO $W^\pm Z$+jet cross section the scale setting is changed to the one in eq. (19) of ref. [36] at large p_T by activating the option `largeptscales 1`. Note that we choose $Q_0 = 0\,\mathrm{GeV}$ in those equations and the Landau singularity is regulated by freezing the strong coupling and the PDFs for scales below $0.8\,\mathrm{GeV}$. Finally, the option `doublefsr 1` of the POWHEG-BOX, first introduced in ref. [82], is turned on: by doing so, for final state radiation, both $q \to qg$ and $g \to q\bar{q}$ splittings are treated symmetrically for the definition of the starting scale of the shower. This considerably reduces the appearance of spikes in distributions due to events with large weights that pass fiducial cuts after showering. As far as the parton shower is concerned we use PYTHIA8 [83] with standard settings, which implies a global recoil scheme for initial state radiation (`SpaceShower:dipoleRecoil 0`).

2.3 NLO$_\mathrm{EW}$+PS implementation

For the computation of NLO EW corrections we have implemented a separate generator within POWHEG-BOX-RES for $W^\pm Z$ production, which is capable of computing $\mathrm{NLO_{EW}+PS}$, $\mathrm{NLO_{QCD}+PS}$, and combined $\mathrm{NLO_{QCD+EW}+PS}$ corrections, all consistently matched to QCD and QED parton showers for all massive diboson processes. This implementation makes use of the POWHEG-BOX-RES [59] framework which allows for resonance-aware NLO subtraction and matching. Within this framework we construct the relevant resonance information for $W^\pm Z$ production, and use the standard resonance projectors of ref. [59]. Also here we employ tree-level and one-loop amplitudes from OPENLOOPS [73–75]. This generator is essentially equivalent to the ones developed in ref. [57].

2.4 Veto procedure for QCD and QED radiation

In order to match both $\mathrm{NNLO_{QCD}}$ and $\mathrm{NLO_{EW}}$ predictions consistently with QCD and QED parton showers in PYTHIA8 we use a veto procedure similar to the one described in ref. [84] (see appendix D). In particular, we let both the QCD and QED showers radiate in the entire phase space (restricted only by the kinematical bound) by setting

```
pythia.readString("SpaceShower:pTmaxMatch = 2"),
pythia.readString("TimeShower:pTmaxMatch = 2"),
```

which sets the shower starting scale equal to the partonic energy $\sqrt{s}$ of the event. For each showered event we perform an a posteriori check of the shower history and we veto events that are not consistent with the emissions generated by POWHEG at Les Houches Event (LHE) level.

More precisely, when computing $\mathrm{NNLO_{QCD}+PS}$ predictions, we need to restrict the QCD emissions generated by the shower, as commonly done in the POWHEG framework,

while QED radiations remain unconstrained, so that the entire kinematically allowed phase space is covered. In order to do so, once an event is showered we scan all the QCD emissions generated by PYTHIA8, store the hardest transverse momentum p_T^{max} and compare it to the hardness of the QCD emission generated by POWHEG (commonly referred to as `scalup`), whose value is read from the event file. If p_T^{max} is greater than `scalup`, we reject the event and try to shower it again until the above requirement is fulfilled. After 1000 unsuccessful attempts the event is rejected.

For the generation of NLO$_{EW}$+PS predictions the QED shower must be restricted, while QCD radiation is unconstrained. QED emissions can be generated both in the production of the two vector bosons and in their resonance decays. Therefore, the shower has to be vetoed both in the production and in the resonance decays of the vector bosons using different veto scales. To do so, we generate events according to the multiple-radiation scheme (`allrad 1`), first introduced in ref. [76], which allows us to distinguish between the generation of radiation from each QED-singular region of the process at hand. In particular, up to one photon emission can be generated in the production stage through initial-state radiation (ISR) and up to one photon can be radiated from each decaying resonance as final-state radiation (FSR). After the event is showered, we scan the list of QED emissions generated by PYTHIA8 and we store the transverse momenta of the hardest emissions in the three regions. We then construct our veto scales: for the production stage we store the transverse momentum of the photon generated by POWHEG as ISR, while for the two resonances we calculate the transverse momentum of the photon generated at LHE level with respect to the lepton emitter in the centre-of-mass frame of the mother resonance, thus, obtaining two different scales for the two vector bosons. If no photon is produced by POWHEG in a certain region, the corresponding veto scale is set equal to an infra-red cutoff (10^{-3} GeV). For each region we check whether the shower contains QED emissions harder than the constructed veto scale in that region. If that is the case, we veto the event and we try to shower it again. After 1000 attempts, the event is rejected.

2.5 Combination of NNLO QCD and NLO EW corrections

In this paper, NNLO$_{QCD}$+PS and NLO$_{EW}$+PS events are generated and showered with PYTHIA8 separately, and their combination is performed a posteriori at the level of differential distributions.

There is a number of different ways how these combinations of higher-order QCD and EW predictions can be defined. First, the QCD and EW perturbative corrections can either be added or multiplied. In the high-energy regime, i.e. in situations where EW effects are dominated by EW Sudakov logarithms [85, 86], and when the dominant QCD effects arise at scales well below the hard scale, a multiplicative combination should be seen as superior, as such QCD effects factorise with respect to the underlying hard di-boson process. However, this assumption is violated in the phenomenologically relevant situation where the process is dominated by underlying hard vector-boson plus jet topologies with an additional soft vector boson. These configurations are forbidden at LO and lead to $\mathcal{O}(1)$ NLO QCD corrections, known as *giant K-factors* [29, 87]. In this regime a multiplicative combination of QCD and EW effects overestimates the impact of the EW

corrections as those EW corrections determined for the hard diboson process are applied to the hard vector-boson plus jet topologies. In turn, an additive combination will largely underestimate the EW corrections, as in this case no EW corrections are considered for the dominating vector-boson plus jet topologies. As discussed in ref. [31] the average of a multiplicative and additive combination can be considered as a pragmatic estimate in such situations. However, as also pointed out in ref. [31], when one is interested in the hard diboson process, in general it is advisable to avoid such topologies through appropriately defined vetos of hard QCD radiation, ideally defined dynamically in phase space.

Second, in any combination a double-counting of both QCD and QED radiation has to be avoided. In this regard one may choose whether QCD and/or QED emissions in the parton shower are accounted for in both the $\mathrm{NNLO_{QCD}+PS}$ and the $\mathrm{NLO_{EW}+PS}$ calculation, or whether either the QED shower is turned off in the $\mathrm{NNLO_{QCD}+PS}$ calculation, or the QCD shower is turned off in the $\mathrm{NLO_{EW}+PS}$ calculation. Any of these choices is consistent as long as the desired formal accuracy is reached without double counting, namely $\mathrm{NNLO_{QCD}}$ and $\mathrm{NLO_{EW}}$ in the perturbative expansion and leading-logarithmic accuracy in both QCD and QED shower emissions.

In order to distinguish the relevant combination schemes we introduce the following notation: $\mathrm{NNLO_{QCD}^{(QCD,QED)PS}}$ refers to NNLO accuracy in QCD perturbation theory matched to a parton shower that includes both QCD and QED emissions, while $\mathrm{NNLO_{QCD}^{(QCD)PS}}$ corresponds to the same perturbative accuracy but with QED shower turned off. Similarly, we introduce $\mathrm{NLO_{EW}^{(QCD,QED)PS}}$ and $\mathrm{NLO_{EW}^{(QED)PS}}$ for the NLO cross section in the EW expansion with and without QCD shower, respectively, as well as the corresponding symbols at LO with both or either one of the two showers turned on, i.e. $\mathrm{LO^{(QCD,QED)PS}}$, $\mathrm{LO^{(QCD)PS}}$, and $\mathrm{LO^{(QED)PS}}$. Furthermore, we introduce a generic term $\mathrm{\delta N(N)LO_X^{(Y,Z)PS}}$ for the coefficient of the $\mathrm{X = \{QCD, EW\}}$ higher-order correction defined as

$$\mathrm{\delta N(N)LO_X^{(Y,Z)PS} = N(N)LO_X^{(Y,Z)PS} - LO^{(Y,Z)PS}} \,, \tag{2.5}$$

and a multiplicative correction factor $\mathrm{K\text{-}N(N)LO_X^{(Y,Z)PS}}$, which reads

$$\mathrm{K\text{-}N(N)LO_X^{(Y,Z)PS} = N(N)LO_X^{(Y,Z)PS}/LO^{(Y,Z)PS}} \,. \tag{2.6}$$

We also define a corresponding NLO EW correction factor $\mathrm{K\text{-}NLO_{EW}^{(f.o.)}}$ obtained at fixed-order with MATRIX+OPENLOOPS

$$\mathrm{K\text{-}NLO_{EW}^{(f.o.)} = NLO_{EW}^{(f.o.)}/LO^{(f.o)}} \,. \tag{2.7}$$

Adopting these notations, we introduce the following schemes to combine NNLO QCD and NLO EW corrections matched to QCD and QED parton showers:

additive schemes:

$$1. \ \text{NNLO}_{\text{QCD}}^{\text{(QCD,QED)PS}} + \delta\text{NLO}_{\text{EW}}^{\text{(QCD,QED)PS}} = \text{NNLO}_{\text{QCD+EW}}^{\text{(QCD,QED)PS}} \tag{2.8}$$

$$2. \ \text{NNLO}_{\text{QCD}}^{\text{(QCD,QED)PS}} + \delta\text{NLO}_{\text{EW}}^{\text{(QED)PS}} \tag{2.9}$$

$$3. \ \text{NLO}_{\text{EW}}^{\text{(QCD,QED)PS}} + \delta\text{NNLO}_{\text{QCD}}^{\text{(QCD)PS}} \tag{2.10}$$

multiplicative schemes:

$$4. \ \text{NNLO}_{\text{QCD}}^{\text{(QCD,QED)PS}} \times \text{K-NLO}_{\text{EW}}^{\text{(QCD,QED)PS}} = \text{NNLO}_{\text{QCD}\times\text{EW}}^{\text{(QCD,QED)PS}} \tag{2.11}$$

$$5. \ \text{NNLO}_{\text{QCD}}^{\text{(QCD,QED)PS}} \times \text{K-NLO}_{\text{EW}}^{\text{(QED)PS}} \tag{2.12}$$

$$6. \ \text{NLO}_{\text{EW}}^{\text{(QCD,QED)PS}} \times \text{K-NNLO}_{\text{QCD}}^{\text{(QCD)PS}} \tag{2.13}$$

$$7. \ \text{NNLO}_{\text{QCD}}^{\text{(QCD)PS}} \times \text{K-NLO}_{\text{EW}}^{\text{(f.o.)}}, \tag{2.14}$$

where for the first and fourth combination we introduced the dedicated short-hand notations $\text{NNLO}_{\text{QCD+EW}}^{\text{(QCD,QED)PS}}$ and $\text{NNLO}_{\text{QCDxEW}}^{\text{(QCD,QED)PS}}$, respectively. In the result section we will consider these combination schemes and study which of them are more appropriate than others based on their ability to describe relevant distributions in the most accurate way. We note that there is a double counting of terms beyond accuracy in the additive combination schemes, which are due to, e.g., configurations in which the NLO EW contribution produces two gluons by showering, which double-count configurations in which the NNLO QCD contribution produces e.g. a photon by showering. There is no such double counting in the multiplicative schemes, therefore the differences between multiplicative and additive schemes are indicative of the size of these (beyond accuracy) double-counting terms.

3 Phenomenological results

In the following we study phenomenological results for $W^{\pm}Z$ at NNLO_{QCD} and NLO_{EW} accuracy matched to parton showers. For brevity and without loss of generality, we focus on the process

$$pp \rightarrow \mu^+ \nu_\mu e^+ e^- , \tag{3.1}$$

but all qualitative conclusions apply also to the case of the charged conjugated process with an intermediate negatively charged W boson as well as to same-flavour leptonic final states. Of course, when comparing to ATLAS data [9] in section 3.4 we consider both charges in the final state, i.e. $pp \rightarrow \mu^{\pm} \nu_\mu e^+ e^-$, and account for all relevant leptonic final states.

3.1 Input parameters and setup

We present results for proton-proton collisions at the LHC with a center-of-mass energy of 13 TeV. The complex-mass scheme [60, 88] is employed throughout and the electroweak (EW) inputs are chosen according to their PDG values [89]: $G_{\text{F}} = 1.16639 \times 10^{-5}\,\text{GeV}^{-2}$, $m_{\text{W}} = 80.385\,\text{GeV}$, $\Gamma_{\text{W}} = 2.0854\,\text{GeV}$, $m_{\text{Z}} = 91.1876\,\text{GeV}$, $\Gamma_{\text{Z}} = 2.4952\,\text{GeV}$, $m_H = 125\,\text{GeV}$

and $\Gamma_H = 0.00407\,\text{GeV}$. The on-shell mass and width of the top-quark are set to $m_t = 173.2\,\text{GeV}$ and $\Gamma_t = 1.347878\,\text{GeV}$. All other EW parameters are determined through the G_μ scheme, in particular by computing the EW coupling as [75]

$$\alpha_{G_\mu} = \frac{\sqrt{2}}{\pi} \, G_\text{F} |(m_\text{W}^2 - i\Gamma_\text{W} m_\text{W}) \sin^2\theta_\text{W}|\,, \tag{3.2}$$

and the EW mixing angle as

$$\cos^2\theta_\text{W} = \frac{m_\text{W}^2 - i\Gamma_\text{W} m_\text{W}}{m_\text{Z}^2 - i\Gamma_\text{Z} m_\text{Z}}\,. \tag{3.3}$$

As PDFs we use the five-flavour NNPDF3.1 [90] NNLO set with $\alpha_s = 0.118$, specifically the `NNPDF31_nnlo_as_0118_luxqed` set [91–93]. The central factorization and renormalization scales are set as discussed in section 2.2 for the MiNNLO$_\text{PS}$ $W^\pm Z$ generator. For the NLO$_\text{EW}$+PS calculation and fixed-order NNLO$_\text{QCD}$ results we set them as

$$\mu_\text{F} = \mu_\text{R} = \frac{1}{2}\left(\sqrt{m_{e^+e^-}^2 + p_{\text{T},e^+e^-}^2} + \sqrt{m_{\mu\nu_\mu}^2 + p_{\text{T},\mu\nu_\mu}^2}\right)\,, \tag{3.4}$$

where $m_{e^+e^-}$ and p_{T,e^+e^-} ($m_{\mu\nu_\mu}$ and $p_{\text{T},\mu\nu_\mu}$) are the invariant mass and the transverse momentum of the reconstructed Z boson (W boson), respectively. Scale uncertainties in all cases are estimated via seven-point scale variation, where μ_F and μ_R are varied around their central values by a factor of two in either direction, with the constraint $0.5 \le \mu_\text{R}/\mu_\text{F} \le 2$. When NNLO$_\text{QCD}$+PS and NLO$_\text{EW}$+PS results are combined, as described in section 2.5, scale variations are assumed to be correlated. Hence, the construction of multiplicative EW correction factors is almost scale independent, up to relative corrections of order α due to μ_F variations.

For all predictions matched to a parton shower presented in this paper we make use of Pythia8 [83] with the Monash 2013 tune [94] (`py8tune 14` in the input card). To validate our calculation, we compare NNLO$_\text{QCD}$+PS and NLO$_\text{EW}$+PS results at LHE level to NNLO$_\text{QCD}$ and NLO$_\text{EW}$ fixed-order predictions obtained with Matrix [20, 31].

In order to prevent charged resonances to radiate photons and photons to branch into lepton- or quark-pairs, we set the two flags `TimeShower:QEDshowerByOther` and `TimeShower:QEDshowerByGamma` to `off`. The former is not to spoil the NLO accuracy of the resonance shape in W-decays. We define dressed leptons by adding to the four-momentum of a charged lepton ℓ the four-momenta of all photons within a distance $\Delta R_{\ell\gamma} = \sqrt{\Delta\phi_{\ell\gamma}^2 + \Delta\eta_{\ell\gamma}^2} < 0.1$, starting from the smallest $R_{\ell\gamma}$ among all lepton-photon combinations, and removing any recombined photons from the list of final-state particles.

When validating our calculation and studying different combinations of QCD and EW corrections matched to QCD and QED parton showering, we consider two different setups: an inclusive one, referred to as `inclusive setup`, with just a mass window for the Z boson, which avoids the photon-pole singularity, and one with a set of fiducial cuts referred to as `fiducial setup`. These setups are summarized in table 1. The `fiducial setup` corresponds to the one used in the ATLAS analyses of ref. [7] and ref. [9], and is the default setup implemented in the Matrix code for $W^\pm Z$ production. Finally, when

	inclusive setup	fiducial setup
Z-mass window	$66\,\mathrm{GeV} < m_{e^+e^-} < 116\,\mathrm{GeV}$	$|m_{e^+e^-} - m_{\mathrm{Z}}| < 10\,\mathrm{GeV}$
lepton cuts		$p_{T,e^\pm} > 15\,\mathrm{GeV}, \quad p_{\mathrm{T},\mu} > 20\,\mathrm{GeV},$ $|\eta_\ell| < 2.5, \quad m_{\mathrm{T,W}} > 30\,\mathrm{GeV},$ $\Delta R_{e^+e^-} > 0.2, \quad \Delta R_{e^\pm\mu} > 0.3$

Table 1. Inclusive and fiducial cuts used to define the phase space regions of the `inclusive setup` and the `fiducial setup` [7]. Note that $e^\pm$ and μ refer to dressed leptons.

comparing to ATLAS data in section 3.4, we exploit the corresponding RIVET routines [95] provided on the `HEPdata` webpage [96] to obtain the distributions in the fiducial volume defined by the recent ATLAS analysis of ref. [9].[1]

For simplicity we do not include effects due to hadronization or multi-particle interactions (MPI) anywhere, but in the comparison against the recent ATLAS results in section 3.4.

3.2 Validation against fixed-order predictions

We start by separately validating our $\mathrm{NNLO_{QCD}}$+PS and $\mathrm{NLO_{EW}}$+PS calculations by comparing results at the LHE level to fixed-order predictions from MATRIX+OPENLOOPS.

3.2.1 NNLO QCD

In figure 2 we show the comparison of $\mathrm{NNLO_{QCD}}$+PS predictions (blue, solid) at the LHE level obtained with the MINNLO$_{\mathrm{PS}}$ $W^\pm Z$ generator to fixed-order $\mathrm{NNLO_{QCD}}$ predictions (red, dashed) for a selection of distributions in the `inclusive setup`. Specifically, we display the distributions in the azimuthal difference between the leading and subleading charged lepton ($\Delta\phi_{\ell_1\ell_2}$), the rapidity of the leading charged lepton (y_{ℓ_1}), the invariant mass of the three charged leptons ($m_{3\ell}$), the invariant mass ($m_{\mu\nu_\mu}$) and the transverse momentum ($p_{\mathrm{T},\mu\nu_\mu}$) of the reconstructed W boson, and the missing transverse momentum ($p_{\mathrm{T,miss}}$). In all plots, the main frame shows the distribution of the cross section in the respective variable, while the lower panel shows the bin-by-bin ratio of all curves to the MINNLO$_{\mathrm{PS}}$ result.

As can be seen, for all distributions MINNLO$_{\mathrm{PS}}$ predictions agree nicely with the fixed-order $\mathrm{NNLO_{QCD}}$ reference result within the perturbative uncertainties at NNLO. Also, the size of the uncertainty bands are very similar between the two calculations. We would like to stress that no one-to-one correspondence between the two predictions is to be expected as they differ by higher-order terms, both due to different choices in the treatment of terms beyond accuracy and due to different scale settings.

We note that we have considered a large number of differential observables and that we just show a representative selection of them here. For all observables inclusive over

---

[1]In our analysis, used for the results presented in section 3.3, we have defined the transverse mass of the W boson in table 1 as $m_{\mathrm{T,W}} = \sqrt{(E_{\mathrm{T},\mu} + E_{\mathrm{T},\nu_\mu})^2 - p_{\mathrm{T},\mu\nu_\mu}^2}$ with $E_{\mathrm{T},x}^2 = m_x^2 + p_{\mathrm{T},x}^2$. The Rivet analysis, employed for the results presented in section 3.4, uses the same definition but sets the mass of the dressed leptons to zero in this formula.
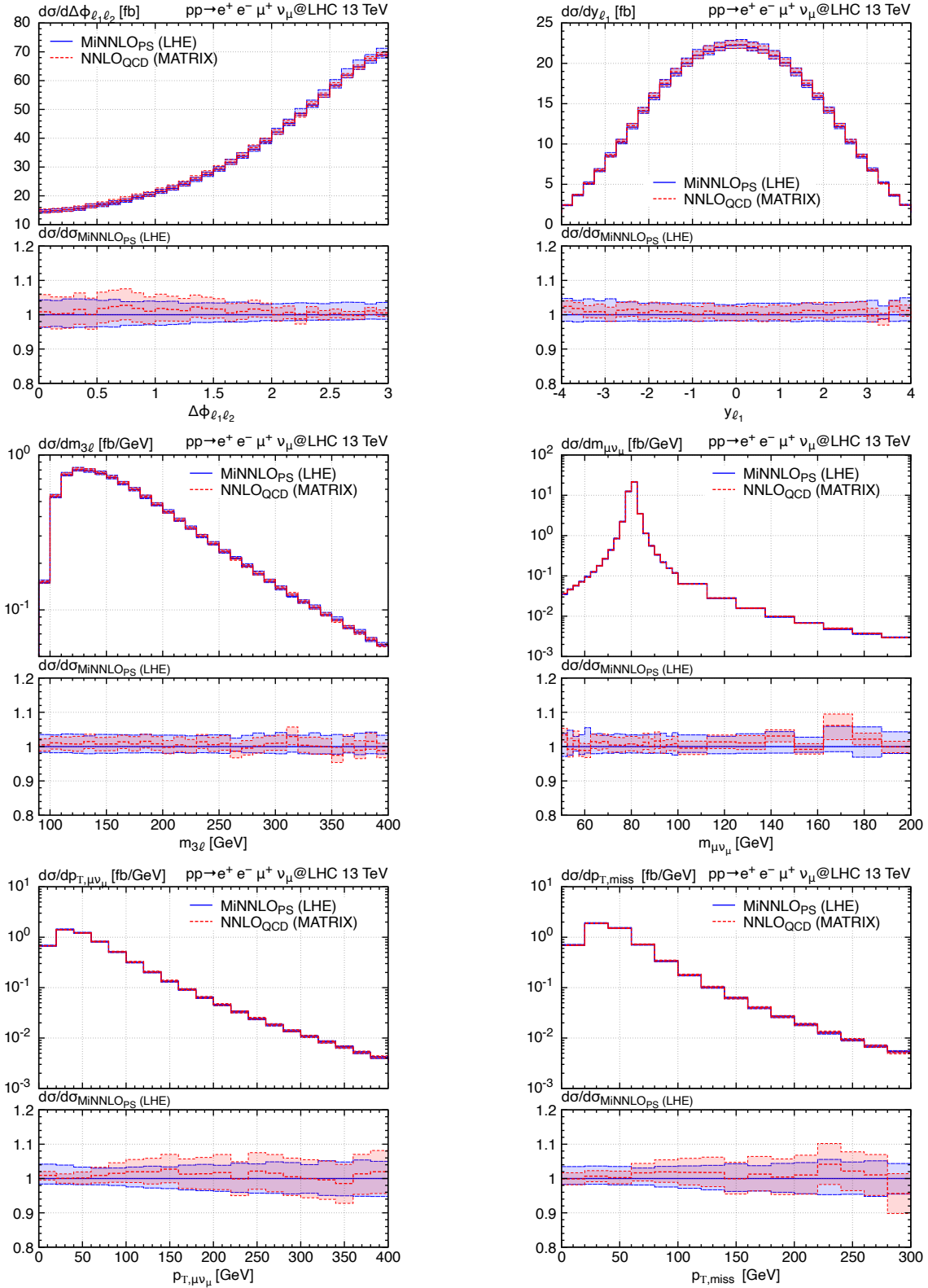
Figure 2. Comparison of MiNNLO$_{PS}$ (blue, solid) and fixed-order NNLO$_{QCD}$ (red, dashed) predictions for W^+Z production in the `inclusive setup`.

QCD radiation, which are genuinely NNLO$_{QCD}$-accurate, M<small>I</small>NNLO$_{PS}$ and fixed-order NNLO$_{QCD}$ results are in excellent agreement within the respective scale uncertainties. This comparison validates the NNLO$_{QCD}$ accuracy of our M<small>I</small>NNLO$_{PS}$ generator, which we will use in the following sections for phenomenological studies in combination with higher-order EW effects.

3.2.2 NLO EW

Figure 3 validates our P<small>OWHEG</small> NLO$_{EW}$ predictions at LHE level against fixed-order NLO$_{EW}$ results for the same set of observables discussed in the previous section in the `inclusive setup`. In this case, the two predictions do have a one-to-one correspondence in the hard region and differ only by the contribution of the P<small>OWHEG</small> Sudakov, which correctly distributes the first photon emission as needed for the subsequent matching of the NLO$_{EW}$ results at LHE level to the parton shower. As a result, the P<small>OWHEG</small> NLO$_{EW}$ (LHE) and fixed-order NLO$_{EW}$ curves are essentially identical up to numerical fluctuations in the tails of the distributions. Moreover, also the size of the perturbative uncertainties, which correspond essentially to LO in QCD, of either prediction is practically identical.

Also in this case we have examined a large number of different differential distributions, finding perfect agreement between the two predictions for all NLO$_{EW}$-accurate observables that are inclusive over photon radiation. Therefore, we consider our NLO$_{EW}$+PS generator fully validated as well, so that we can move on to considering phenomenological results for the combination of NNLO$_{QCD}$+PS and NLO$_{EW}$+PS predictions in the next section.

3.3 Parton-shower matched results

In this section we present results for $W^\pm Z$ production at NNLO$_{QCD}$ and NLO$_{EW}$, both matched to QCD and/or QED parton showers. We consider different ways for the combination of NNLO$_{QCD}$+PS and NLO$_{EW}$(+PS) predictions, as introduced in section 2.5. In order to distinguish between relevant EW and QED effects, we compare these different combinations of NNLO$_{QCD}$+PS and NLO$_{EW}$+PS predictions to dedicated approximations with lower formal accuracy, which include the pure NNLO$_{QCD}$+PS predictions with and without QED showering, i.e. NNLO$_{QCD}^{(QCD,QED)_{PS}}$ and NNLO$_{QCD}^{(QCD)_{PS}}$, respectively, as well as a multiplicative combination of NNLO$_{QCD}$+PS results with a fixed-order EW K-factor obtained through M<small>ATRIX</small>+O<small>PEN</small>L<small>OOPS</small>, as defined in eq. (2.14).

Unless otherwise stated, all figures throughout this section are organized as follows: the main frame shows NNLO$_{QCD}^{(QCD,QED)_{PS}}$ (blue, dashed), NNLO$_{QCD+EW}^{(QCD,QED)_{PS}}$ (magenta, long-dashed) and NNLO$_{QCDxEW}^{(QCD,QED)_{PS}}$ (green, solid) predictions. In the first ratio panel these curves are normalized to the NNLO$_{QCD}^{(QCD,QED)_{PS}}$ prediction to visualize the EW effects. In addition, the NNLO$_{QCD}^{(QCD)_{PS}}$ result (red, dash-dotted), i.e. NNLO QCD matched to a QCD shower but without QED shower, is shown. In the second ratio inset the additive and multiplicative QCD-EW combinations are normalized to the additive one to better display their differences. Additionally, in this second ratio panel we show the NNLO$_{QCD}^{(QCD)_{PS}} \times$ K-NLO$_{EW}^{(f.o.)}$ combination (brown, dash-dotted), and, where explicitly stated, further combinations as defined in section 2.5. In all plots the uncertainty bands
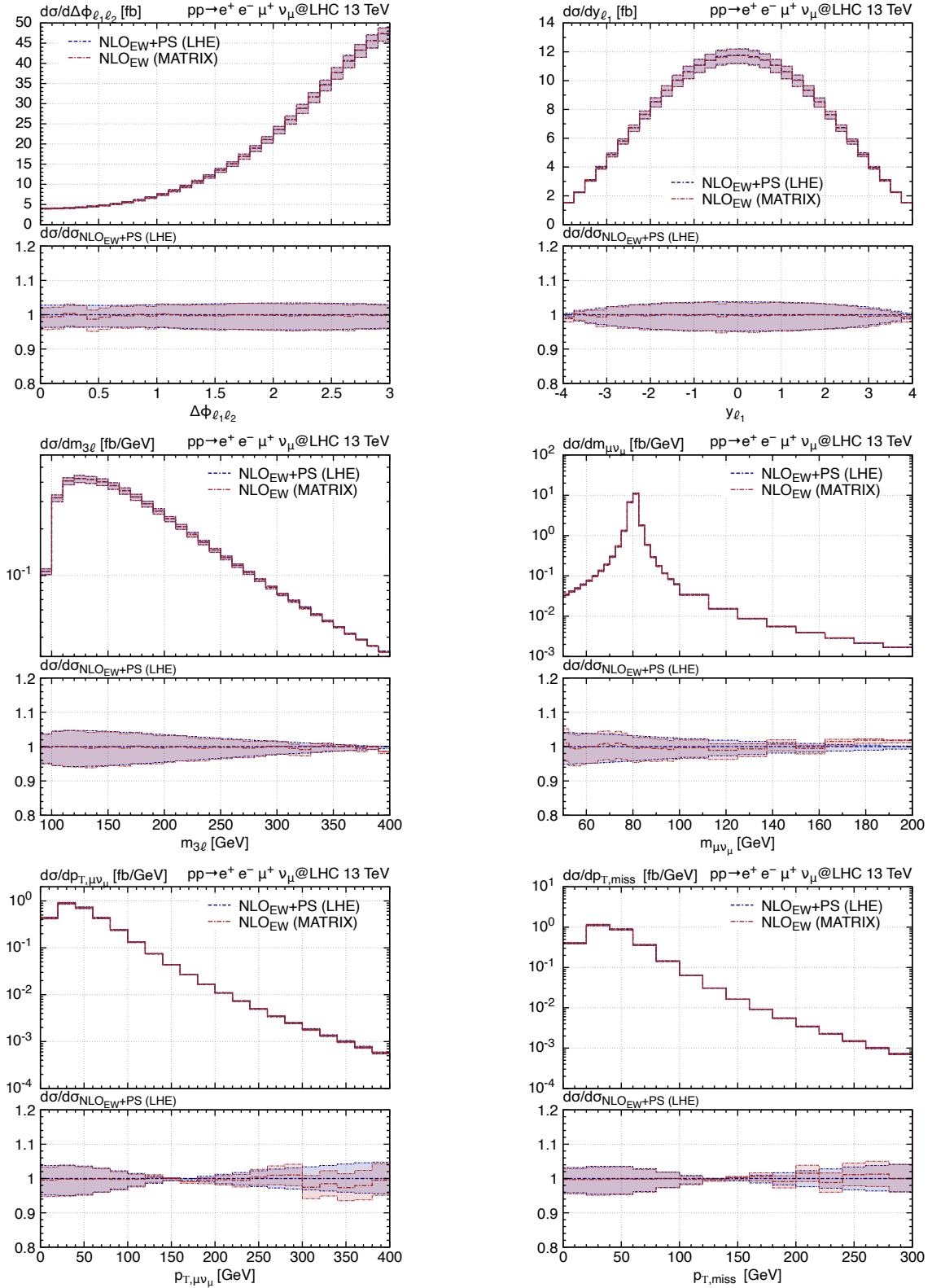
Figure 3. Comparison of NLO$_{\text{EW}}$+PS (dark blue, double-dash dotted) and fixed-order NLO$_{\text{EW}}$ (brown, dash-dotted) predictions for W^+Z production in the `inclusive setup`.
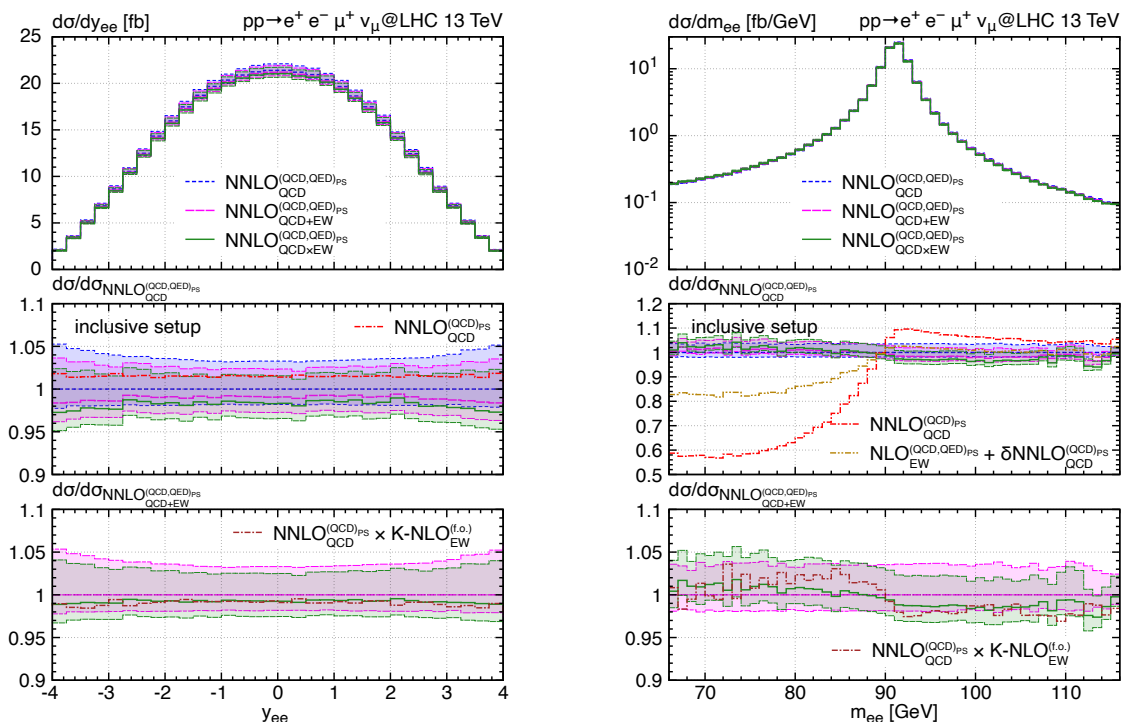
Figure 4. Differential distributions of the dilepton rapidity originating from the Z-boson (left) and of the corresponding dilepton invariant mass (right) in W^+Z production in the `inclusive setup` at NNLO_{QCD} combined with NLO_{EW} matched to parton showers for different combination schemes. See text for details.

correspond to seven-point scale variations, keeping scale variations in the QCD and EW predictions correlated. We stress that multiplicative EW correction factors are essentially scale independent, and that for all combination schemes the uncertainties are dominated by NNLO QCD scale variations.

We start our discussion of the numerical results in figure 4 with observables focusing on the reconstructed Z-boson, namely the rapidity (y_{ee}) and the invariant mass (m_{ee}) of the lepton-pair associated with the Z boson in the `inclusive setup`. Looking at the y_{ee} distribution in figure 4 (left) we observe scale-uncertainty bands with upper and lower edges at the level of $+3$–5% and -2–3%, respectively, in all shown predictions. EW corrections are smaller than these QCD scale variations and show hardly any shape effects, as expected from this observable that is inclusive with respect to QED radiation. Indeed, comparing the $\text{NNLO}_{\text{QCD}}^{(\text{QCD})\text{PS}}$ prediction against the $\text{NNLO}_{\text{QCD}}^{(\text{QCD,QED})\text{PS}}$ one indicates that pure QED effects are at the level of -1–2%, and an additional -2–3% of weak origin is found when comparing further against the NLO EW-matched $\text{NNLO}_{\text{QCD+EW}}^{(\text{QCD,QED})\text{PS}}$ or $\text{NNLO}_{\text{QCDxEW}}^{(\text{QCD,QED})\text{PS}}$ predictions, which in turn agree at the one percent level. We also observe that the $\text{NNLO}_{\text{QCD}}^{(\text{QCD})\text{PS}} \times \text{K-NLO}_{\text{EW}}^{(\text{f.o.})}$ prediction is practically identical with the $\text{NNLO}_{\text{QCDxEW}}^{(\text{QCD,QED})\text{PS}}$ one, which implies that multiple photon emissions (beyond the first one) do not have a relevant impact here.

Looking at the m_{ee} distribution in figure 4 (right), the observations are different: there are large effects from collinear QED radiation which shift events from above the Breit-Wigner peak to below the peak. These effects are entirely absent in the $\mathrm{NNLO}_{\mathrm{QCD}}^{(\mathrm{QCD})\mathrm{PS}}$ prediction showing deviations of up to 40% compared to the $\mathrm{NNLO}_{\mathrm{QCD}}^{(\mathrm{QCD,QED})\mathrm{PS}}$ prediction including effects from the QED shower. The observed shape of the corrections due to these collinear QED effects is qualitatively very similar to the well-known NLO EW corrections to neutral-current Drell-Yan (plus jet) production for dressed leptons [97–99]. It is interesting to notice that the NNLO+PS QCD prediction with a QED shower, i.e $\mathrm{NNLO}_{\mathrm{QCD}}^{(\mathrm{QCD,QED})\mathrm{PS}}$, provides an excellent approximation of this distribution with respect to the full $\mathrm{NNLO}_{\mathrm{QCD+EW}}^{(\mathrm{QCD,QED})\mathrm{PS}}$ and $\mathrm{NNLO}_{\mathrm{QCDxEW}}^{(\mathrm{QCD,QED})\mathrm{PS}}$ combinations, see central ratio panel in figure 4 (right). In the same panel, we also included the central $\mathrm{NLO}_{\mathrm{EW}}^{(\mathrm{QCD,QED})\mathrm{PS}} + \delta\mathrm{NNLO}_{\mathrm{QCD}}^{(\mathrm{QCD})\mathrm{PS}}$ result (brown, dash-double-dotted) in order to show that it does not provide a suitable prediction for the m_{ee} distribution, as it misses important mixed QED-QCD effects (although beyond accuracy) originating from QED corrections relative to the NNLO QCD contribution, and, thus, it can be discarded as a useful combination from the list in eq. (2.14). Comparing the $\mathrm{NNLO}_{\mathrm{QCDxEW}}^{(\mathrm{QCD,QED})\mathrm{PS}}$ prediction with the $\mathrm{NNLO}_{\mathrm{QCD}}^{(\mathrm{QCD})\mathrm{PS}} \times \mathrm{K\text{-}NLO}_{\mathrm{EW}}^{(\mathrm{f.o.})}$ combination we observe agreement at the 1–2% level, see lower ratio panel in figure 4 (right). On the one hand, this further validates the employed resonance-aware matching of the EW corrections with QED parton-shower radiation within POWHEG-BOX-RES, and, on the other hand, indicates only a mild impact of multi-photon radiation beyond the first emission, despite the sizable QED effects due to collinear photon radiation. Furthermore, given the very small observed differences between the additive and multiplicative combination schemes at the level of 1–2%, i.e. well below scale uncertainties, we consider the difference between the two combination schemes a reliable estimate of remaining mixed QCD-EW effects for the observable at hand.

For the rest of the discussion we turn to high-energy tails of differential distributions in figures 5–7, which are relevant in particular for new-physics searches at the energy frontier. For all observables under consideration we show results in both the `inclusive setup` and the `fiducial setup`, as defined in table 1. In order to render the high-energy tails visible, in these figures we employ a logarithmic scale (and binning) on the x-axis. Moreover, we have added the central $\mathrm{NNLO}_{\mathrm{QCD}}^{(\mathrm{QCD,QED})\mathrm{PS}} \times \mathrm{K\text{-}NLO}_{\mathrm{EW}}^{(\mathrm{QED})\mathrm{PS}}$ predictions (orange, dash-double-dotted) in the lower ratio insets for comparison.

We start the discussion of high-energy observables with the distribution in the missing transverse momentum ($p_{\mathrm{T,miss}}$), for which corresponding plots in the `inclusive setup` (left) and in the `fiducial setup` (right) are shown in figure 5. Here, by and large, both the `inclusive setup` and the `fiducial setup` show very similar results. Comparing the $\mathrm{NNLO}_{\mathrm{QCD}}^{(\mathrm{QCD})\mathrm{PS}}$ and $\mathrm{NNLO}_{\mathrm{QCD}}^{(\mathrm{QCD,QED})\mathrm{PS}}$ curves in the first ratio panel we find percent level effects from QED emissions in the entire considered $p_{\mathrm{T,miss}}$ range. By contrast, the NLO EW corrections are significantly enhanced at large $p_{\mathrm{T,miss}}$ values due to the appearance of EW Sudakov logarithms. Corrections in the multiplicative combination scheme $\mathrm{NNLO}_{\mathrm{QCDxEW}}^{(\mathrm{QCD,QED})\mathrm{PS}}$ reach about -15% at $p_{\mathrm{T,miss}} = 500\,\mathrm{GeV}$, while in the additive scheme $\mathrm{NNLO}_{\mathrm{QCD+EW}}^{(\mathrm{QCD,QED})\mathrm{PS}}$ they reach about -4% for the same value of $p_{\mathrm{T,miss}}$. These differences can be explained due to large NLO QCD corrections plaguing the $p_{\mathrm{T,miss}}$

distribution. These large QCD effects are known as 'giant K-factors' as discussed in section [2.5](#) and originate from hard vector-boson plus jet topologies with an additional soft vector boson. As discussed in ref. [31] in this situation it is reasonable to consider the average between $\text{NNLO}_{\text{QCDxEW}}^{\text{(QCD,QED)PS}}$ and $\text{NNLO}_{\text{QCD+EW}}^{\text{(QCD,QED)PS}}$ as nominal prediction, and their spread can be interpreted as $\mathcal{O}\left(\alpha_S \alpha\right)$ uncertainty band. Looking at the lower ratio inset, we observe that qualitatively the fixed-order NLO_{EW} K-factor approximation and the parton-shower matched $\text{NNLO}_{\text{QCDxEW}}^{\text{(QCD,QED)PS}}$ and $\text{NNLO}_{\text{QCD}}^{\text{(QCD,QED)PS}} \times \text{K-NLO}_{\text{EW}}^{\text{(QED)PS}}$ predictions follow the same trend. However, at low $p_{\text{T,miss}}$ one can observe differences of the fixed-order approximation up to about 5%, which are present only in the `fiducial setup` and thus induced by the fiducial cuts. In this regime these differences are in fact larger than the remaining scale uncertainties, indicating the relevance of using the NLO EW parton-shower matched computations instead of the fixed-order approximation. In the deep tail of the $p_{\text{T,miss}}$ distribution, on the other hand, we see that our nominal $\text{NNLO}_{\text{QCDxEW}}^{\text{(QCD,QED)PS}}$ prediction shows a somewhat smaller EW Sudakov suppression than predicted at fixed order and by the $\text{NNLO}_{\text{QCD}}^{\text{(QCD,QED)PS}} \times \text{K-NLO}_{\text{EW}}^{\text{(QED)PS}}$ combination, where the NLO EW K-factor is computed turning on only the QED shower, but without QCD shower. We have verified that these differences can be traced back to aforementioned giant QCD K-factor effects, which are generated by the QCD emissions in the partons-shower matching of the $\text{NNLO}_{\text{QCDxEW}}^{\text{(QCD,QED)PS}}$ combination. Indeed, after applying a suitable (dynamical) veto against QCD radiation to select configurations where both vector bosons are sufficiently hard, as suggested in ref. [31], we found the two parton-shower matched predictions to be practically indistinguishable.

Next in figure [6](#) we turn to the discussion of the distributions in the transverse momentum of the leading (p_{T,ℓ_1}) and the subleading (p_{T,ℓ_2}) charged leptons. These distributions constitute important experimental observables for both new-physics searches and for constraining anomalous couplings. By and large, the qualitative behaviour of these distributions and the relative corrections is very similar to the one observed for the $p_{\text{T,miss}}$ distribution: NNLO QCD scale uncertainties increase from the level of few percent in the bulk to about 10% in the tail of the transverse-momentum distributions, while the EW corrections yield important shape distortions with increasing negative corrections in the high transverse-momentum tail. At low transverse momenta, fiducial cuts induce important effects that can be described appropriately only by using the parton-shower matched QCD-EW combinations. At high transverse momenta, our nominal multiplicative $\text{NNLO}_{\text{QCDxEW}}^{\text{(QCD,QED)PS}}$ combination features smaller NLO EW corrections than predicted at fixed order and the $\text{NNLO}_{\text{QCD}}^{\text{(QCD,QED)PS}} \times \text{K-NLO}_{\text{EW}}^{\text{(QED)PS}}$ result. We recall that this difference is induced by giant QCD corrections created by the QCD shower in the $\text{NNLO}_{\text{QCDxEW}}^{\text{(QCD,QED)PS}}$ combination, which affect the NLO EW K-factor. Indeed, for the p_{T,ℓ_2} distribution, which is less affected by giant K-factor effects, the three multiplicative predictions in the lower ratio panel are much closer to one another than in the case of the p_{T,ℓ_1} distribution. At variance with the $p_{\text{T,miss}}$ distribution, we observe non-trivial QED effects at low transverse momenta. These effects are visible both comparing the $\text{NNLO}_{\text{QCD}}^{\text{(QCD)PS}}$ and $\text{NNLO}_{\text{QCD}}^{\text{(QCD,QED)PS}}$ curves in the central ratio panel and when comparing $\text{NNLO}_{\text{QCDxEW}}^{\text{(QCD,QED)PS}}$ with the fixed-order approximation in the lower ratio panel.
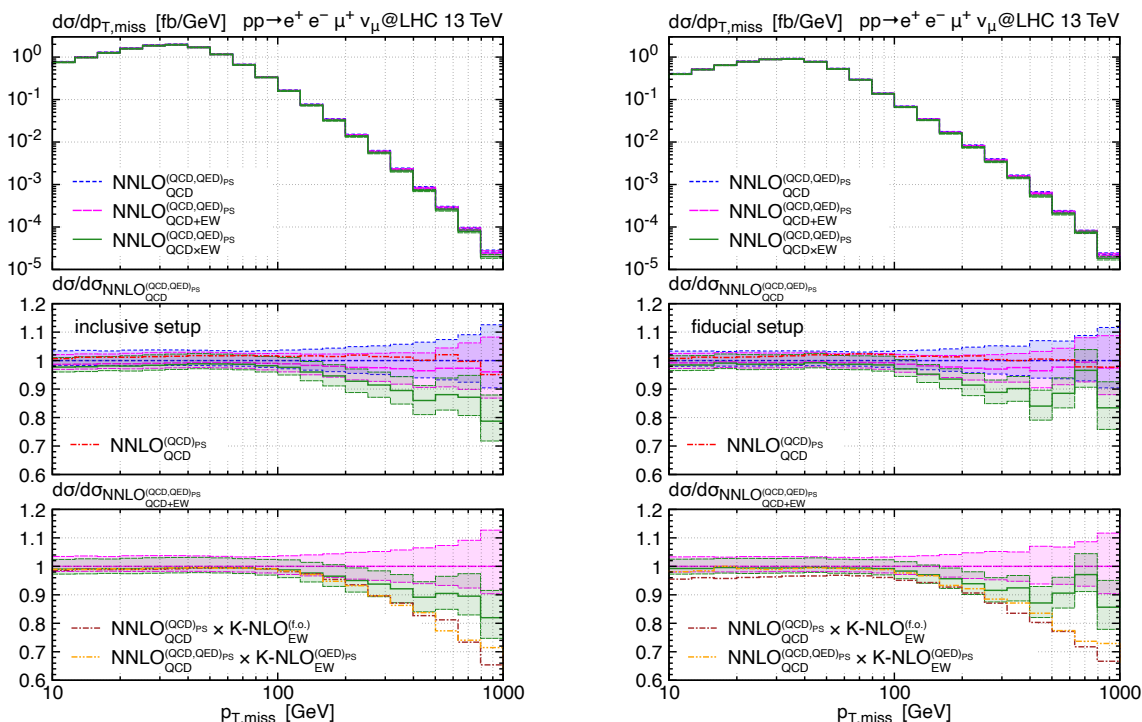
Figure 5. Differential distributions in the missing transverse-momentum $p_{\mathrm{T,miss}}$ in W^+Z production in the `inclusive setup` (left) and `fiducial setup` (right). See text for details.

Finally, in figure 7 we consider the invariant-mass distributions of the three charged final-state leptons $(m_{3\ell})$, which can be seen as a proxy for the (unobservable) invariant mass of the full $W^{\pm}Z$ system. Also for this observable the EW corrections are negative and increase in the high-energy tail due to the appearance of EW Sudakov logarithms. It is interesting to notice that the EW corrections substantially increase as soon as fiducial cuts are applied. Indeed, when moving from the `inclusive setup` to the `fiducial setup`, negative EW effects at invariant-mass values of $\sim 2\,\mathrm{TeV}$ increase from about -10% to about -20–30%, rendering the inclusion of EW corrections crucial in such high-energy phase-space regions. The origin of this effect can be explained as follows: in the `inclusive setup`, the high-$m_{3\ell}$ region is populated by very forward leptons at large rapidities. In this regime, not all Mandelstam invariants s_{ij} are large, resulting in a suppression of the double Sudakov logarithms $\ln^2(|\hat{s}_{ij}|/M_W^2)$. In the `fiducial setup`, the very forward regime of the leptons is removed by their rapidity requirements, resulting in the expected EW Sudakov enhancement. We also point out that the $m_{3\ell}$ distribution is not plagued by giant QCD K-factor effects. Therefore, the $\mathrm{NNLO}_{\mathrm{QCD \times EW}}^{(\mathrm{QCD,QED})_{\mathrm{PS}}}$ and the $\mathrm{NNLO}_{\mathrm{QCD}}^{(\mathrm{QCD,QED})_{\mathrm{PS}}} \times$ K-$\mathrm{NLO}_{\mathrm{EW}}^{(\mathrm{QED})_{\mathrm{PS}}}$ parton-shower combinations, as well as the fixed-order approximation of the EW corrections, practically coincide with one another in the $m_{3\ell}$ tail.

We note that in our numerical results presented here we have not included any results for the $\mathrm{NNLO}_{\mathrm{QCD}}^{(\mathrm{QCD,QED})_{\mathrm{PS}}} + \delta\mathrm{NLO}_{\mathrm{EW}}^{(\mathrm{QED})_{\mathrm{PS}}}$ combination, because we have not found any meaningful differences with respect to the $\mathrm{NNLO}_{\mathrm{QCD+EW}}^{(\mathrm{QCD,QED})_{\mathrm{PS}}}$ curves shown in the presented
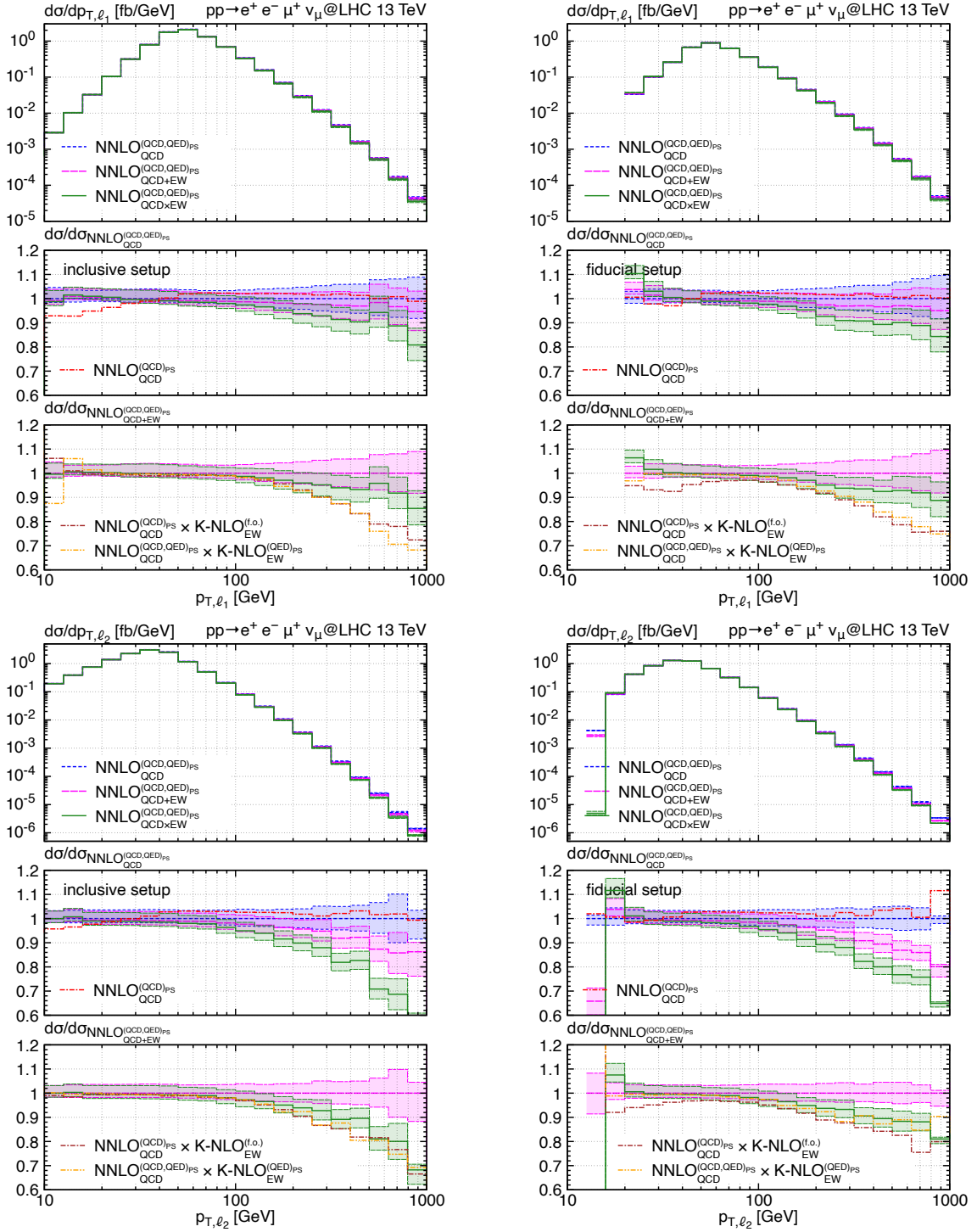
Figure 6. Differential distributions in the leading lepton transverse momentum (p_{T,ℓ_1}) (top) and subleading lepton transverse momentum (p_{T,ℓ_2}) in W^+Z production in the `inclusive setup` (left) and `fiducial setup` (right). See text for details.
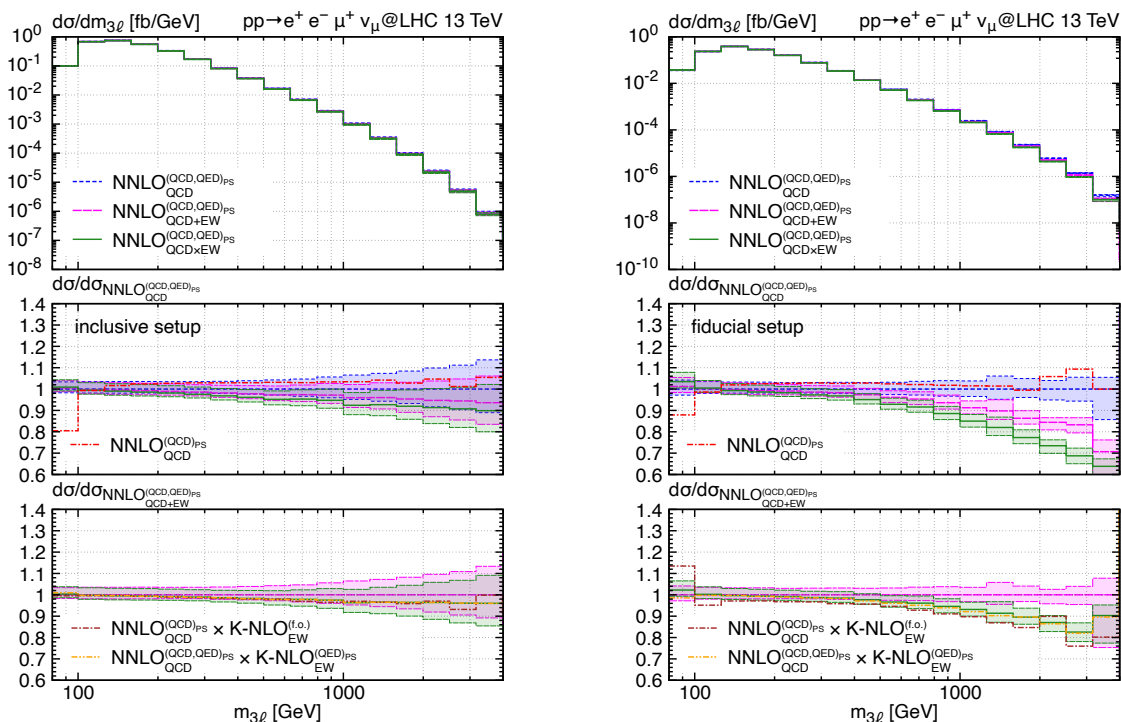
Figure 7. Differential distributions in the invariant mass of the three final-state leptons in W^+Z production in the `inclusive setup` (left) and `fiducial setup` (right). See text for details.

figures, and we consider both approaches equally appropriate as an additive combination. Similarly, the $\mathrm{NLO}_{\mathrm{EW}}^{(\mathrm{QCD},\mathrm{QED})_{\mathrm{PS}}} \times \text{K-NNLO}_{\mathrm{QCD}}^{(\mathrm{QCD})_{\mathrm{PS}}}$ combination yields very similar results to the $\mathrm{NNLO}_{\mathrm{QCD}\times\mathrm{EW}}^{(\mathrm{QCD},\mathrm{QED})_{\mathrm{PS}}}$ predictions, including the sensitivity to giant QCD K-factors generated by the QCD shower for certain observables (which are again alleviated through a proper veto against QCD radiation). Consequently, we also refrain from showing any $\mathrm{NNLO}_{\mathrm{QCD}}^{(\mathrm{QCD},\mathrm{QED})_{\mathrm{PS}}} \times \text{K-NLO}_{\mathrm{EW}}^{(\mathrm{QED})_{\mathrm{PS}}}$ results.

3.4 Comparison to data

Finally, we compare our default MiNNLO$_{\mathrm{PS}}$ predictions, which correspond the multiplicative combination of NNLO QCD and NLO EW corrections, defined as $\mathrm{NNLO}_{\mathrm{QCD}\times\mathrm{EW}}^{(\mathrm{QCD},\mathrm{QED})_{\mathrm{PS}}}$ in eq. (2.11), to a recent differential measurement of $W^{\pm}Z$ production performed by the ATLAS collaboration [9]. The fiducial phase space is defined in section 3.1. To facilitate this comparison, we employ the corresponding RIVET routines provided on the HEPdata webpage [96] for the analysis of ref. [9]. The differential distributions measured in ref. [9] correspond to the averaged $W^{\pm}Z$ cross section of all combinations of electrons and muons in the final state. Thus, the $W^{\pm}Z$ cross section for the same-flavour channels ($e^+e^-e^{\pm}\nu_e$, $\mu^+\mu^-\mu^{\pm}\nu_\mu$) and different-flavour channels ($e^+e^-\mu^{\pm}\nu_\mu$, $e^+e^-\mu^{\pm}\nu_\mu$) are summed and divided by four, i.e. by the total number of channels. For simplicity, our MiNNLO$_{\mathrm{PS}}$ predictions rely on the different-flavour channel only, in which case the W and the Z boson can be un-
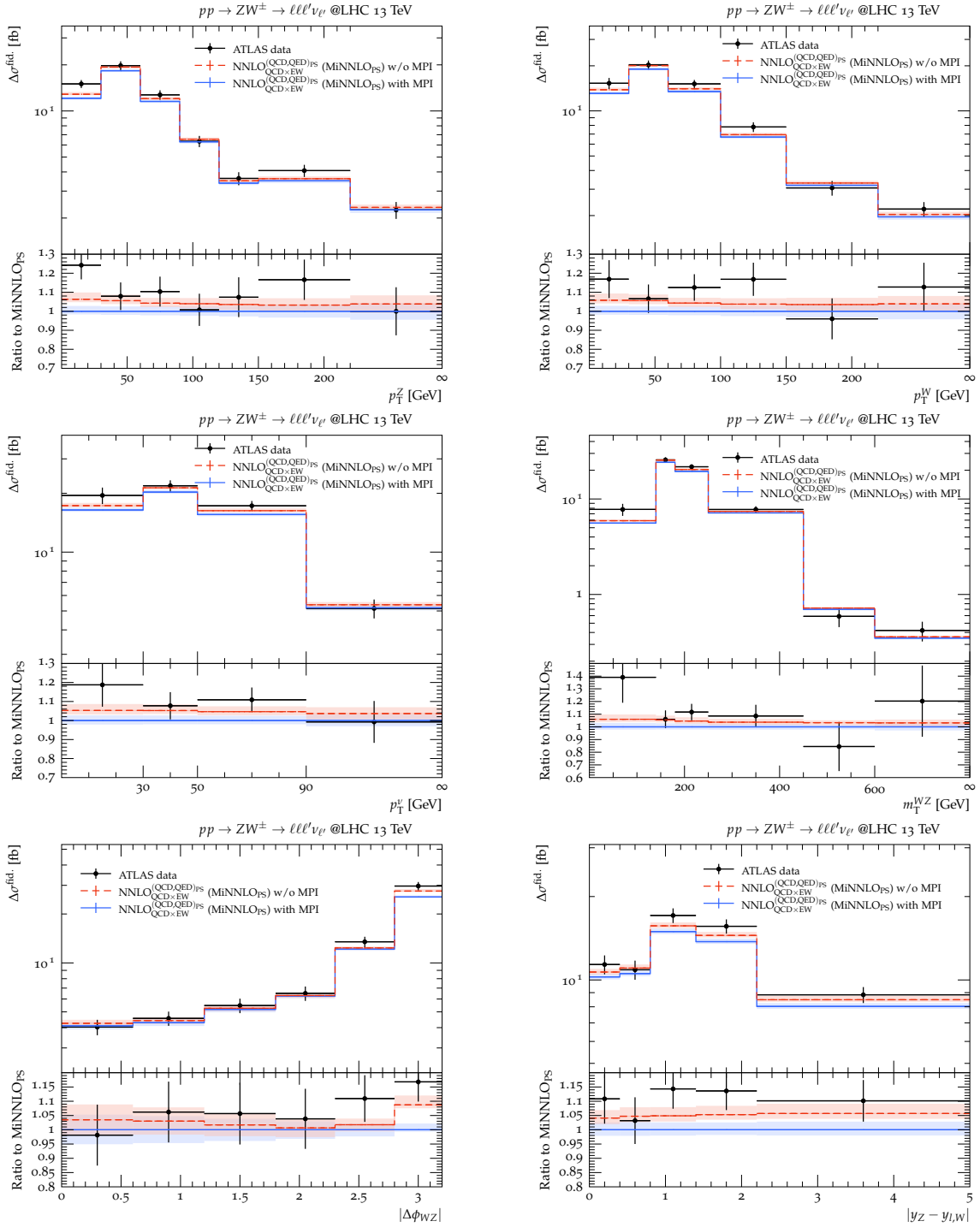
Figure 8. Comparison of our default MiNNLO$_{\text{PS}}$ prediction NNLO$_{\text{QCDxEW}}^{(\text{QCD,QED})_{\text{PS}}}$ with MPI effects (blue, solid) and without (red, dashed) against the ATLAS data from the analysis [9].

ambiguously reconstructed.[2] Indeed, using the different-flavour result for the same-flavour channel has been shown to be an excellent approximation [19], especially when the vector bosons are reconstructed according to the "resonant-shape" identification procedure, which yields a very high performance in reliably reconstructing the W and Z bosons. The ATLAS analysis of ref. [9] that is considered here is based exactly on this kind of reconstruction.

In figure 8 we show the distributions in the transverse momentum of the reconstructed Z boson ($p_{\mathrm{T},Z}$), of the reconstructed W boson ($p_{\mathrm{T},W}$) and of the neutrino ($p_{\mathrm{T},\nu}$), i.e. the missing transverse momentum, the transverse mass of the $W^{\pm}Z$ system ($m_{\mathrm{T},WZ}$), defined as

$$m_{\mathrm{T},WZ} = \sqrt{\left(\sum_{i=1}^{4} p_{\mathrm{T},i}\right)^2 - p_{\mathrm{T},WZ}^2}\,, \tag{3.5}$$

where the sum runs over the three charged leptons and the neutrino, as well as the difference in the azimuthal angle between the reconstructed Z and W bosons ($\Delta\phi_{WZ}$) and the absolute rapidity difference between the reconstructed Z boson and the charged lepton coming from the W decay ($|y_Z - y_{\ell_W}|$). The main frame of all plots in figure 8 shows the absolute cross section per bin for the data and our default prediction, while the lower panel shows the ratio to MiNNLO$_{\mathrm{PS}}$. The last bin in all kinematically unbounded distributions shall be understood as an overflow bin, which is indicated by the infinity symbol on the x axis of its right edge. We note that, except for $\Delta\phi_{WZ}$ (where $\Delta\phi_{WZ} = \pi$ at LO), all distributions are defined already at LO in the Born phase space and are therefore genuinely NNLO QCD and NLO EW accurate. In these distributions, our MiNNLO$_{\mathrm{PS}}$ predictions provide a remarkable agreement with data. This is true both in the bulk region of the cross section, where NNLO QCD corrections are vital, and in the tails of the distributions, where NLO EW corrections become relevant. It is interesting to notice, however, that MPI effects are relatively large, lowering the predictions by about 5% and, overall, leading to a slightly worse agreement with data. With remaining scale uncertainties of only a few percent, the theory predictions can be regarded as extremely precise. On the contrary, the experimental errors have not reached (yet) a comparable level of accuracy with the given statistics of $36.1\,\mathrm{fb}^{-1}$, which can nevertheless be expected to change once the full Run 2 data is considered and, even more so, once Run 3 data becomes available in the future.

As anticipated, the $\Delta\phi_{WZ}$ distribution is filled for $\Delta\phi_{WZ} < \pi$ only upon inclusion of higher-order corrections, since this region requires a recoil for the $W^{\pm}Z$ system, for instance by a jet. As a result, this distribution is effectively only NLO QCD accurate at low $\Delta\phi_{WZ}$, which is also reflected by the slightly enlarged scale-uncertainty band. Moreover, around the $\Delta\phi_{WZ} = \pi$ threshold the distribution becomes sensitive to soft-gluon effects, which are accounted for by the matching to the parton shower. Despite these caveats, the agreement between the predicted and measured $\Delta\phi_{WZ}$ distribution is excellent and within at most one standard deviation for all bins.

---

[2]We stress again that the codes developed in this work can simulate both different-flavour and same-flavour events.

4   Conclusions

In this paper we have presented the first calculation of NNLO QCD corrections matched to parton showers for $W^\pm Z$ production at the LHC. We consistently combined this calculation with NLO EW corrections that we also matched to parton showers. This is the first time such accuracy is reached in the simulation of a LHC process. This is achieved via two separate implementations within the POWHEG-BOX-RES code, consisting of one MiNNLO$_{PS}$ $W^\pm Z$ generator and one POWHEG generator for $W^\pm Z$ production including both NLO QCD and NLO EW corrections.

Our results have been validated against fixed-order calculations in NNLO QCD and NLO EW obtained from MATRIX. For observables related to the colour-singlet final state, which are inclusive over radiation and not sensitive to soft-gluon effects, our MiNNLO$_{PS}$ predictions are fully compatible with fixed-order NNLO QCD predictions within scale uncertainties. As far as our POWHEG NLO EW implementation is concerned, the NLO EW cross sections have been shown to be essentially identical in the relevant phase space regions to their fixed-order counterparts obtained with MATRIX+OPENLOOPS.

Phenomenological results have been discussed in detail for various combinations of NNLO QCD and NLO EW predictions. In particular, we have investigated different additive and multiplicative combination approaches. In these combinations we consistently included and/or excluded QCD and QED emissions in the shower matching in certain parts of our combined NNLO QCD and NLO EW accurate calculation, avoiding any double counting while preserving the desired accuracy. We have considered a number of distributions where different physical effects become relevant, both in the fully inclusive phase space and in presence of fiducial cuts.

We find that QED effects are crucial for observables related to the dressed charged leptons due to recoil effects, which can not be fully reabsorbed by the dressing. This is particularly important in the line-shape distribution of the reconstructed Z boson, but also below the peak in other invariant mass distributions as well as at small transverse momenta of the charged leptons. We observed that in most cases the full tower of QED emissions as generated by the QED shower is well approximated when considering only the first photon emission through a fixed-order calculation. However, in certain cases differences up to 10% remain.

In the bulk of the cross sections (away from high-energy tails), we find that just accounting for EW effects through a QED shower applied only to the NNLO QCD MiNNLO$_{PS}$ predictions already serves as a very good approximation. Instead, full NLO EW corrections are most important in the high-energy tails of distributions, where they lead to a strong suppression of the cross section due to large EW Sudakov logarithms. We argued that, generally speaking, a multiplicative scheme is more suitable for describing high-energy regions of phase space. Indeed, since EW Sudakov logarithms are expected to largely factorize with respect to QCD corrections, a multiplicative scheme provides a better approximation of the missing mixed QCD-EW contributions. However, this general assumption does not hold for distributions plagued by giant QCD K-factors, which are dominated by $W^\pm Z$+jet topologies. In fact, in such a situation also the computation of an NLO EW K-factor in a parton-shower matched calculation can be affected by whether

QCD shower emissions are taken into account or not, as those emissions can create giant QCD correction effects in the high-energy tails. However, by selecting phase-space configurations involving two hard vector bosons, e.g. through appropriate (dynamical) jet-veto prescriptions, any giant K-factor issues can be avoided. Moreover, we have shown that in high-energy tails EW corrections obtained at NLO+PS can be well approximated by using a NLO EW K-factor computed at fixed order. This justifies the application of NLO EW K-factors on QCD predictions, which have been widely used by the LHC collaborations. However, when applying these factors on showered predictions, QED shower effects have to be turned off in order to avoid a double counting of QED radiation. Nevertheless, we also observed that fiducial cuts can affect the size of NLO EW corrections in the bulk region of the cross section, rendering parton-shower matched NLO EW predictions important for precision measurements.

Not least, we have employed our default predictions including NNLO QCD and NLO EW corrections in a direct comparison to recent ATLAS data at 13 TeV. We find remarkable agreement between theory predictions and experimental data for all observables. At the moment, the experimental accuracy is still limited by statistical uncertainties for the considered $36.1\,\mathrm{fb}^{-1}$ analysis. However, with scale uncertainties of only few percent our MiNNLO$_{\rm PS}$ predictions will facilitate high-precision studies for $W^{\pm}Z$ production in the future. The Monte Carlo generators developed in this work will be made publicly available within the Powheg-Box-Res framework.

Finally, in order to control remaining QCD-EW mixed uncertainties in observables subject to giant K-factors, and in order to directly produce NNLO QCD and NLO EW accurate events, instead of combining such predictions a posteriori at the level of distributions, we will consider suitable extensions of the MiNNLO$_{\rm PS}$ method in the future. This will allow to simulate fully differential events for $W^{\pm}Z$ production and other colour-singlet processes that are NNLO QCD and NLO EW accurate.

Acknowledgments

References

[1] D.E. Morrissey, T. Plehn and T.M.P. Tait, *Physics searches at the LHC*, *Phys. Rept.* **515** (2012) 1 [arXiv:0912.3259] [INSPIRE].

[2] CDF collaboration, *Measurement of the WZ cross section and triple gauge couplings in $p\bar{p}$ collisions at $\sqrt{s} = 1.96$ TeV*, *Phys. Rev. D* **86** (2012) 031104 [arXiv:1202.6629] [INSPIRE].

[3] D0 collaboration, *A measurement of the WZ and ZZ production cross sections using leptonic final states in $8.6\,fb^{-1}$ of $p\bar{p}$ collisions*, *Phys. Rev. D* **85** (2012) 112005 [arXiv:1201.5652] [INSPIRE].

[4] ATLAS collaboration, *Measurement of WZ production in proton-proton collisions at $\sqrt{s} = 7$ TeV with the ATLAS detector*, *Eur. Phys. J. C* **72** (2012) 2173 [arXiv:1208.1390] [INSPIRE].

[5] CMS collaboration, *Measurement of the WZ production cross section in pp collisions at $\sqrt{s} = 7$ and 8 TeV and search for anomalous triple gauge couplings at $\sqrt{s} = 8$ TeV*, *Eur. Phys. J. C* **77** (2017) 236 [arXiv:1609.05721] [INSPIRE].

[6] ATLAS collaboration, *Measurements of $W^{\pm}Z$ production cross sections in pp collisions at $\sqrt{s} = 8$ TeV with the ATLAS detector and limits on anomalous gauge boson self-couplings*, *Phys. Rev. D* **93** (2016) 092004 [arXiv:1603.02151] [INSPIRE].

[7] ATLAS collaboration, *Measurement of the $W^{\pm}Z$ boson pair-production cross section in pp collisions at $\sqrt{s} = 13$ TeV with the ATLAS detector*, *Phys. Lett. B* **762** (2016) 1 [arXiv:1606.04017] [INSPIRE].

[8] CMS collaboration, *Measurement of the WZ production cross section in pp collisions at $\sqrt{s} = 13$ TeV*, *Phys. Lett. B* **766** (2017) 268 [arXiv:1607.06943] [INSPIRE].

[9] ATLAS collaboration, *Measurement of $W^{\pm}Z$ production cross sections and gauge boson polarisation in pp collisions at $\sqrt{s} = 13$ TeV with the ATLAS detector*, *Eur. Phys. J. C* **79** (2019) 535 [arXiv:1902.05759] [INSPIRE].

[10] CMS collaboration, *Measurement of the inclusive and differential WZ production cross sections, polarization angles, and triple gauge couplings in pp collisions at $\sqrt{s} = 13$ TeV*, *JHEP* **07** (2022) 032 [arXiv:2110.11231] [INSPIRE].

[11] J. Ohnemus, *An order-α_s calculation of hadronic $W^{\pm}Z$ production*, *Phys. Rev. D* **44** (1991) 3477 [INSPIRE].

[12] J. Ohnemus, *Hadronic ZZ, W^-W^+, and $W^{\pm}Z$ production with QCD corrections and leptonic decays*, *Phys. Rev. D* **50** (1994) 1931 [hep-ph/9403331] [INSPIRE].

[13] J.M. Campbell and R.K. Ellis, *An update on vector boson pair production at hadron colliders*, *Phys. Rev. D* **60** (1999) 113006 [hep-ph/9905386] [INSPIRE].

[14] L.J. Dixon, Z. Kunszt and A. Signer, *Vector boson pair production in hadronic collisions at order α_s: lepton correlations and anomalous couplings*, *Phys. Rev. D* **60** (1999) 114037 [hep-ph/9907305] [INSPIRE].

[15] J.M. Campbell, R.K. Ellis and C. Williams, *Vector boson pair production at the LHC*, *JHEP* **07** (2011) 018 [arXiv:1105.0020] [INSPIRE].

[16] A. Denner and G. Pelliccioli, *NLO QCD predictions for doubly-polarized WZ production at the LHC*, *Phys. Lett. B* **814** (2021) 136107 [arXiv:2010.07149] [INSPIRE].

[17] F. Campanario, C. Englert, S. Kallweit, M. Spannowsky and D. Zeppenfeld, *NLO QCD corrections to WZ+jet production with leptonic decays*, *JHEP* **07** (2010) 076 [arXiv:1006.0390] [INSPIRE].

[18] M. Grazzini, S. Kallweit, D. Rathlev and M. Wiesemann, *$W^{\pm}Z$ production at hadron colliders in NNLO QCD*, *Phys. Lett. B* **761** (2016) 179 [arXiv:1604.08576] [INSPIRE].

[19] M. Grazzini, S. Kallweit, D. Rathlev and M. Wiesemann, *$W^{\pm}Z$ production at the LHC: fiducial cross sections and distributions in NNLO QCD*, *JHEP* **05** (2017) 139 [arXiv:1703.09065] [INSPIRE].

[20] M. Grazzini, S. Kallweit and M. Wiesemann, *Fully differential NNLO computations with MATRIX*, *Eur. Phys. J. C* **78** (2018) 537 [arXiv:1711.06631] [INSPIRE].

[21] J.M. Campbell, R.K. Ellis and S. Seth, *Non-local slicing approaches for NNLO QCD in MCFM*, *JHEP* **06** (2022) 002 [arXiv:2202.07738] [INSPIRE].

[22] M. Grazzini, S. Kallweit, D. Rathlev and M. Wiesemann, *Transverse-momentum resummation for vector-boson pair production at NNLL+NNLO*, *JHEP* **08** (2015) 154 [arXiv:1507.02565] [INSPIRE].

[23] S. Kallweit, E. Re, L. Rottoli and M. Wiesemann, *Accurate single- and double-differential resummation of colour-singlet processes with MATRIX+RADISH: $W^{+}W^{-}$ production at the LHC*, *JHEP* **12** (2020) 147 [arXiv:2004.07720] [INSPIRE].

[24] M. Wiesemann, L. Rottoli and P. Torrielli, *The $Z\gamma$ transverse-momentum spectrum at $NNLO+N^3LL$*, *Phys. Lett. B* **809** (2020) 135718 [arXiv:2006.09338] [INSPIRE].

[25] P.F. Monni, E. Re and P. Torrielli, *Higgs transverse-momentum resummation in direct space*, *Phys. Rev. Lett.* **116** (2016) 242001 [arXiv:1604.02191] [INSPIRE].

[26] W. Bizon, P.F. Monni, E. Re, L. Rottoli and P. Torrielli, *Momentum-space resummation for transverse observables and the Higgs $p_{\perp}$ at $N^3LL+NNLO$*, *JHEP* **02** (2018) 108 [arXiv:1705.09127] [INSPIRE].

[27] P.F. Monni, L. Rottoli and P. Torrielli, *Higgs transverse momentum with a jet veto: a double-differential resummation*, *Phys. Rev. Lett.* **124** (2020) 252001 [arXiv:1909.04704] [INSPIRE].

[28] A. Bierweiler, T. Kasprzik and J.H. Kühn, *Vector-boson pair production at the LHC to $O(\alpha^3)$ accuracy*, *JHEP* **12** (2013) 071 [arXiv:1305.5402] [INSPIRE].

[29] J. Baglio, L.D. Ninh and M.M. Weber, *Massive gauge boson pair production at the LHC: a next-to-leading order story*, *Phys. Rev. D* **88** (2013) 113005 [*Erratum ibid.* **94** (2016) 099902] [arXiv:1307.4331] [INSPIRE].

[30] B. Biedermann, A. Denner and L. Hofer, *Next-to-leading-order electroweak corrections to the production of three charged leptons plus missing energy at the LHC*, *JHEP* **10** (2017) 043 [arXiv:1708.06938] [INSPIRE].

[31] M. Grazzini, S. Kallweit, J.M. Lindert, S. Pozzorini and M. Wiesemann, *NNLO QCD + NLO EW with Matrix+OpenLoops: precise predictions for vector-boson pair production*, *JHEP* **02** (2020) 087 [arXiv:1912.00068] [INSPIRE].

[32] K. Hamilton, P. Nason, C. Oleari and G. Zanderighi, *Merging $H/W/Z + 0$ and 1 jet at NLO with no merging scale: a path to parton shower + NNLO matching*, *JHEP* **05** (2013) 082 [arXiv:1212.4504] [INSPIRE].

[33] S. Alioli, C.W. Bauer, C. Berggren, F.J. Tackmann, J.R. Walsh and S. Zuberi, *Matching fully differential NNLO calculations and parton showers*, *JHEP* **06** (2014) 089 [arXiv:1311.0286] [INSPIRE].

[34] S. Höche, Y. Li and S. Prestel, *Drell-Yan lepton pair production at NNLO QCD with parton showers*, *Phys. Rev. D* **91** (2015) 074015 [arXiv:1405.3607] [INSPIRE].

[35] P.F. Monni, P. Nason, E. Re, M. Wiesemann and G. Zanderighi, *MiNNLO$_{PS}$: a new method to match NNLO QCD to parton showers*, *JHEP* **05** (2020) 143 [*Erratum ibid.* **02** (2022) 031] [arXiv:1908.06987] [INSPIRE].

[36] P.F. Monni, E. Re and M. Wiesemann, *MiNNLO$_{PS}$: optimizing $2 \to 1$ hadronic processes*, *Eur. Phys. J. C* **80** (2020) 1075 [arXiv:2006.04133] [INSPIRE].

[37] K. Hamilton, P. Nason, E. Re and G. Zanderighi, *NNLOPS simulation of Higgs boson production*, *JHEP* **10** (2013) 222 [arXiv:1309.0017] [INSPIRE].

[38] S. Höche, Y. Li and S. Prestel, *Higgs-boson production through gluon fusion at NNLO QCD with parton showers*, *Phys. Rev. D* **90** (2014) 054011 [arXiv:1407.3773] [INSPIRE].

[39] A. Karlberg, E. Re and G. Zanderighi, *NNLOPS accurate Drell-Yan production*, *JHEP* **09** (2014) 134 [arXiv:1407.2940] [INSPIRE].

[40] S. Alioli, C.W. Bauer, C. Berggren, F.J. Tackmann and J.R. Walsh, *Drell-Yan production at NNLL'+NNLO matched to parton showers*, *Phys. Rev. D* **92** (2015) 094020 [arXiv:1508.01475] [INSPIRE].

[41] S. Alioli et al., *Matching NNLO predictions to parton showers using N^3LL color-singlet transverse momentum resummation in geneva*, *Phys. Rev. D* **104** (2021) 094020 [arXiv:2102.08390] [INSPIRE].

[42] W. Astill, W. Bizon, E. Re and G. Zanderighi, *NNLOPS accurate associated HW production*, *JHEP* **06** (2016) 154 [arXiv:1603.01620] [INSPIRE].

[43] W. Astill, W. Bizoń, E. Re and G. Zanderighi, *NNLOPS accurate associated HZ production with $H \to b\bar{b}$ decay at NLO*, *JHEP* **11** (2018) 157 [arXiv:1804.08141] [INSPIRE].

[44] S. Alioli, A. Broggio, S. Kallweit, M.A. Lim and L. Rottoli, *Higgsstrahlung at NNLL'+NNLO matched to parton showers in GENEVA*, *Phys. Rev. D* **100** (2019) 096016 [arXiv:1909.02026] [INSPIRE].

[45] S. Zanoli, M. Chiesa, E. Re, M. Wiesemann and G. Zanderighi, *Next-to-next-to-leading order event generation for VH production with $H \to b\bar{b}$ decay*, *JHEP* **07** (2022) 008 [arXiv:2112.04168] [INSPIRE].

[46] U. Haisch, D.J. Scott, M. Wiesemann, G. Zanderighi and S. Zanoli, *NNLO event generation for $pp \to Zh \to \ell^+\ell^- b\bar{b}$ production in the SM effective field theory*, *JHEP* **07** (2022) 054 [arXiv:2204.00663] [INSPIRE].

[47] S. Alioli et al., *Precise predictions for photon pair production matched to parton showers in GENEVA*, *JHEP* **04** (2021) 041 [arXiv:2010.10498] [INSPIRE].

[48] A. Gavardi, C. Oleari and E. Re, *NNLO+PS Monte Carlo simulation of photon pair production with MiNNLO$_{PS}$*, *JHEP* **09** (2022) 061 [arXiv:2204.12602] [INSPIRE].

[49] D. Lombardi, M. Wiesemann and G. Zanderighi, *Advancing MiNNLO$_{PS}$ to diboson processes: $Z\gamma$ production at NNLO+PS*, *JHEP* **06** (2021) 095 [arXiv:2010.10478] [INSPIRE].

[50] D. Lombardi, M. Wiesemann and G. Zanderighi, *Anomalous couplings in $Z\gamma$ events at NNLO+PS and improving $\nu\bar{\nu}\gamma$ backgrounds in dark-matter searches*, *Phys. Lett. B* **824** (2022) 136846 [arXiv:2108.11315] [INSPIRE].

[51] S. Alioli et al., *Next-to-next-to-leading order event generation for Z boson pair production matched to parton shower*, *Phys. Lett. B* **818** (2021) 136380 [arXiv:2103.01214] [INSPIRE].

[52] L. Buonocore, G. Koole, D. Lombardi, L. Rottoli, M. Wiesemann and G. Zanderighi, *ZZ production at nNNLO+PS with MiNNLO_{PS}*, *JHEP* **01** (2022) 072 [arXiv:2108.05337] [INSPIRE].

[53] E. Re, M. Wiesemann and G. Zanderighi, *NNLOPS accurate predictions for W^+W^- production*, *JHEP* **12** (2018) 121 [arXiv:1805.09857] [INSPIRE].

[54] D. Lombardi, M. Wiesemann and G. Zanderighi, *W^+W^- production at NNLO+PS with MINNLO_{PS}*, *JHEP* **11** (2021) 230 [arXiv:2103.12077] [INSPIRE].

[55] J. Mazzitelli, P.F. Monni, P. Nason, E. Re, M. Wiesemann and G. Zanderighi, *Next-to-next-to-leading order event generation for top-quark pair production*, *Phys. Rev. Lett.* **127** (2021) 062001 [arXiv:2012.14267] [INSPIRE].

[56] J. Mazzitelli, P.F. Monni, P. Nason, E. Re, M. Wiesemann and G. Zanderighi, *Top-pair production at the LHC with MINNLO_{PS}*, *JHEP* **04** (2022) 079 [arXiv:2112.12135] [INSPIRE].

[57] M. Chiesa, C. Oleari and E. Re, *NLO QCD+NLO EW corrections to diboson production matched to parton shower*, *Eur. Phys. J. C* **80** (2020) 849 [arXiv:2005.12146] [INSPIRE].

[58] E. Bothmann, D. Napoletano, M. Schönherr, S. Schumann and S.L. Villani, *Higher-order EW corrections in ZZ and ZZj production at the LHC*, *JHEP* **06** (2022) 064 [arXiv:2111.13453] [INSPIRE].

[59] T. Ježo and P. Nason, *On the treatment of resonances in next-to-leading order calculations matched to a parton shower*, *JHEP* **12** (2015) 065 [arXiv:1509.09071] [INSPIRE].

[60] A. Denner, S. Dittmaier, M. Roth and L.H. Wieders, *Electroweak corrections to charged-current $e^+e^- \to 4$ fermion processes: technical details and further results*, *Nucl. Phys. B* **724** (2005) 247 [*Erratum ibid.* **854** (2012) 504] [hep-ph/0505042] [INSPIRE].

[61] F. Caola, K. Melnikov, R. Röntsch and L. Tancredi, *QCD corrections to ZZ production in gluon fusion at the LHC*, *Phys. Rev. D* **92** (2015) 094028 [arXiv:1509.06734] [INSPIRE].

[62] F. Caola, M. Dowling, K. Melnikov, R. Röntsch and L. Tancredi, *QCD corrections to vector boson pair production in gluon fusion including interference effects with off-shell Higgs at the LHC*, *JHEP* **07** (2016) 087 [arXiv:1605.04610] [INSPIRE].

[63] S. Alioli, F. Caola, G. Luisoni and R. Röntsch, *ZZ production in gluon fusion at NLO matched to parton-shower*, *Phys. Rev. D* **95** (2017) 034042 [arXiv:1609.09719] [INSPIRE].

[64] M. Grazzini, S. Kallweit, M. Wiesemann and J.Y. Yook, *ZZ production at the LHC: NLO QCD corrections to the loop-induced gluon fusion channel*, *JHEP* **03** (2019) 070 [arXiv:1811.09593] [INSPIRE].

[65] M. Grazzini, S. Kallweit, M. Wiesemann and J.Y. Yook, *W^+W^- production at the LHC: NLO QCD corrections to the loop-induced gluon fusion channel*, *Phys. Lett. B* **804** (2020) 135399 [arXiv:2002.01877] [INSPIRE].

[66] M. Grazzini, S. Kallweit, M. Wiesemann and J.Y. Yook, *Four lepton production in gluon fusion: off-shell Higgs effects in NLO QCD*, *Phys. Lett. B* **819** (2021) 136465 [arXiv:2102.08344] [InSPIRE].

[67] S. Alioli, S. Ferrario Ravasio, J.M. Lindert and R. Röntsch, *Four-lepton production in gluon fusion at NLO matched to parton showers*, *Eur. Phys. J. C* **81** (2021) 687 [arXiv:2102.07783] [InSPIRE].

[68] R.W. Brown, D. Sahdev and K.O. Mikaelian, $W^{\pm}Z^0$ *and* $W^{\pm}\gamma$ *pair production in neutrino e, pp, and* $\bar{p}p$ *collisions*, *Phys. Rev. D* **20** (1979) 1164 [InSPIRE].

[69] P. Nason, *A new method for combining NLO QCD with shower Monte Carlo algorithms*, *JHEP* **11** (2004) 040 [hep-ph/0409146] [InSPIRE].

[70] P. Nason and G. Ridolfi, *A positive-weight next-to-leading-order Monte Carlo for Z pair hadroproduction*, *JHEP* **08** (2006) 077 [hep-ph/0606275] [InSPIRE].

[71] S. Frixione, P. Nason and C. Oleari, *Matching NLO QCD computations with parton shower simulations: the POWHEG method*, *JHEP* **11** (2007) 070 [arXiv:0709.2092] [InSPIRE].

[72] S. Alioli, P. Nason, C. Oleari and E. Re, *A general framework for implementing NLO calculations in shower Monte Carlo programs: the POWHEG BOX*, *JHEP* **06** (2010) 043 [arXiv:1002.2581] [InSPIRE].

[73] F. Cascioli, P. Maierhöfer and S. Pozzorini, *Scattering amplitudes with open loops*, *Phys. Rev. Lett.* **108** (2012) 111601 [arXiv:1111.5206] [InSPIRE].

[74] F. Buccioni, S. Pozzorini and M. Zoller, *On-the-fly reduction of open loops*, *Eur. Phys. J. C* **78** (2018) 70 [arXiv:1710.11452] [InSPIRE].

[75] F. Buccioni et al., *OpenLoops 2*, *Eur. Phys. J. C* **79** (2019) 866 [arXiv:1907.13071] [InSPIRE].

[76] T. Ježo, J.M. Lindert, P. Nason, C. Oleari and S. Pozzorini, *An NLO+PS generator for* $t\bar{t}$ *and Wt production and decay including non-resonant and interference effects*, *Eur. Phys. J. C* **76** (2016) 691 [arXiv:1607.04538] [InSPIRE].

[77] T. Gehrmann, A. von Manteuffel and L. Tancredi, *The two-loop helicity amplitudes for* $q\bar{q}' \to V_1V_2 \to 4$ *leptons*, *JHEP* **09** (2015) 128 [arXiv:1503.04812] [InSPIRE].

[78] T. Gehrmann, A. von Manteuffel and L. Tancredi, *The VVAMP project website*, http://vvamp.hepforge.org.

[79] G.P. Salam and J. Rojo, *A Higher Order Perturbative Parton Evolution Toolkit (HOPPET)*, *Comput. Phys. Commun.* **180** (2009) 120 [arXiv:0804.3755] [InSPIRE].

[80] A. Buckley et al., *LHAPDF6: parton density access in the LHC precision era*, *Eur. Phys. J. C* **75** (2015) 132 [arXiv:1412.7420] [InSPIRE].

[81] T. Gehrmann and E. Remiddi, *Numerical evaluation of harmonic polylogarithms*, *Comput. Phys. Commun.* **141** (2001) 296 [hep-ph/0107173] [InSPIRE].

[82] P. Nason and C. Oleari, *Generation cuts and Born suppression in POWHEG*, arXiv:1303.3922 [InSPIRE].

[83] T. Sjöstrand et al., *An introduction to PYTHIA 8.2*, *Comput. Phys. Commun.* **191** (2015) 159 [arXiv:1410.3012] [InSPIRE].

[84] F. Granata, J.M. Lindert, C. Oleari and S. Pozzorini, *NLO QCD+EW predictions for HV and HV + jet production including parton-shower effects*, *JHEP* **09** (2017) 012 [arXiv:1706.03522] [INSPIRE].

[85] A. Denner and S. Pozzorini, *One loop leading logarithms in electroweak radiative corrections. 1. Results*, *Eur. Phys. J. C* **18** (2001) 461 [hep-ph/0010201] [INSPIRE].

[86] E. Accomando, A. Denner and A. Kaiser, *Logarithmic electroweak corrections to gauge-boson pair production at the LHC*, *Nucl. Phys. B* **706** (2005) 325 [hep-ph/0409247] [INSPIRE].

[87] M. Rubin, G.P. Salam and S. Sapeta, *Giant QCD K-factors beyond NLO*, *JHEP* **09** (2010) 084 [arXiv:1006.2144] [INSPIRE].

[88] A. Denner, S. Dittmaier, M. Roth and D. Wackeroth, *Predictions for all processes $e^+e^- \to 4$ fermions $+ \gamma$*, *Nucl. Phys. B* **560** (1999) 33 [hep-ph/9904472] [INSPIRE].

[89] PARTICLE DATA GROUP collaboration, *Review of particle physics*, *PTEP* **2020** (2020) 083C01 [INSPIRE].

[90] NNPDF collaboration, *Parton distributions from high-precision collider data*, *Eur. Phys. J. C* **77** (2017) 663 [arXiv:1706.00428] [INSPIRE].

[91] A. Manohar, P. Nason, G.P. Salam and G. Zanderighi, *How bright is the proton? A precise determination of the photon parton distribution function*, *Phys. Rev. Lett.* **117** (2016) 242002 [arXiv:1607.04266] [INSPIRE].

[92] A.V. Manohar, P. Nason, G.P. Salam and G. Zanderighi, *The photon content of the proton*, *JHEP* **12** (2017) 046 [arXiv:1708.01256] [INSPIRE].

[93] NNPDF collaboration, *Illuminating the photon content of the proton within a global PDF analysis*, *SciPost Phys.* **5** (2018) 008 [arXiv:1712.07053] [INSPIRE].

[94] P. Skands, S. Carrazza and J. Rojo, *Tuning PYTHIA 8.1: the Monash 2013 tune*, *Eur. Phys. J. C* **74** (2014) 3024 [arXiv:1404.5630] [INSPIRE].

[95] C. Bierlich et al., *Robust independent validation of experiment and theory: Rivet version 3*, *SciPost Phys.* **8** (2020) 026 [arXiv:1912.05451] [INSPIRE].

[96] *HEPData website*, https://www.hepdata.net/record/ins1720438.

[97] C.M. Carloni Calame, G. Montagna, O. Nicrosini and A. Vicini, *Precision electroweak calculation of the production of a high transverse-momentum lepton pair at hadron colliders*, *JHEP* **10** (2007) 109 [arXiv:0710.1722] [INSPIRE].

[98] S. Dittmaier and M. Huber, *Radiative corrections to the neutral-current Drell-Yan process in the Standard Model and its minimal supersymmetric extension*, *JHEP* **01** (2010) 060 [arXiv:0911.2329] [INSPIRE].

[99] S. Kallweit, J.M. Lindert, P. Maierhöfer, S. Pozzorini and M. Schönherr, *NLO QCD+EW predictions for V + jets including off-shell vector-boson decays and multijet merging*, *JHEP* **04** (2016) 021 [arXiv:1511.08692] [INSPIRE].